OCTOBER 1995

ECN-C--95-093

PRE-TEST ANALYSES FOR THE NESC1 SPINNING CYLINDER EXPERIMENT

J.H. FOKKENS

The Netherlands Energy Research Foundation ECN is the leading institute in the Netherlands for energy research. ECN carries out basic and applied research in the fields of nuclear energy, fossil fuels, renewable energy sources, policy studies, environmental aspects of energy supply and the development and application of new materials.

ECN employs more than 800 staff. Contracts are obtained from the government and from national and foreign organizations and industries.

ECN's research results are published in a number of report series, each series serving a different public, from contractors to the international scientific world.

The C-series is for contract reports that contain the results of contract research. The contractor's name can be found on page 2.

Het Energieonderzoek Centrum Nederland (ECN) is het centrale instituut voor onderzoek op energiegebied in Nederland. ECN verricht fundamenteel en toegepast onderzoek op het gebied van kernenergie, fossiele-energiedragers, duurzame energie, beleidsstudies, milieuaspecten van de energievoorziening en de ontwikkeling en toepassing van nieuwe materialen.

Bij ECN zijn ruim 800 medewerkers werkzaam. De opdrachten worden verkregen van de overheid en van organisaties en industrieën uit binnen- en buitenland.

De resultaten van het ECN-onderzoek worden neergelegd in diverse rapportenseries, bestemd voor verschillende doelgroepen, van opdrachtgevers tot de internationale wetenschappelijke wereld.

De C-serie is de serie voor contractrapporten. Deze rapporten bevatten de uitkomsten van onderzoek dat in opdracht is uitgevoerd. De opdrachtgever staat vermeld op pagina 2.

Netherlands Energy Research Foundation ECN
P.O. Box 1
NL-1755 ZG Petten
the Netherlands
Telephone : +31 2246 49 49
Fax : +31 2246 44 80

This report is available on remittance of Dfl. 35 to:
ECN, Facility Services,
Petten, the Netherlands
Postbank account No. 3977703.
Please quote the report number.

Energieonderzoek Centrum Nederland
Postbus 1
1755 ZG Petten
Telefoon : (02246) 49 49
Fax : (02246) 44 80

Dit rapport is te verkrijgen door het overmaken van f 35,-- op girorekening 3977703 ten name van:
ECN, Faciliteiten
te Petten
onder vermelding van het rapportnummer.

OCTOBER 1995

KS002046027
R: FI
DE008891838

ECN-C--95-093

DE008891838

PRE-TEST ANALYSES FOR THE NESC1 SPINNING CYLINDER EXPERIMENT

J.H. FOKKENS

Revisions		
1	Final	23 October 1995
A	For review	15 September 1995

Made by J.H. Fokkens 951023	**Approved** B. van der Schaaf 951023	ECN - Nucleaire Energie Toegepaste Mechanica
Checked by H. Braam 25/10/95	**Issued** 23 October 1995	

This work was carried out in the framework of the NESC Structural Analysis Task Group (TG3) of the NESC-1 project.
ECN project number : 1.1716.01.01

ABSTRACT

The spinning cylinder experiment organised by the Network for the Evaluation of Steel Components (NESC) is designed to investigate the cleavage initiation behaviour of both surface breaking and subclad defects in simulated end of life RPV material, exposed to a pressurised thermal shock transient. Pre-test structural integrity assessments are performed by the NESC Structural Analysis Task Group (TG3). The results of these structural integrity assessments are used to determine the design of the experiment and especially the sizes of the introduced defects.

In this report the results of the pre-test analyses performed by the group Applied Mechanics at ECN - Nuclear Energy are described. Elastic as well as elasto-plastic structural analyses are performed for a surface breaking and a subclad defect in a forged cylinder with a 4 mm cladding. The semi elliptical defects have a depth of 40 mm and an aspect ratio of 1 : 3.

CONTENTS

1. INTRODUCTION 5

2. GEOMETRY, MATERIAL PROPERTIES AND LOADING CONDITIONS 7
   - 2.1 Geometry description 7
   - 2.2 Material properties 7
   - 2.3 Loading conditions 8

3. MODEL DESCRIPTION 9
   - 3.1 Mesh layout 9
   - 3.2 Thermal transient model 9
   - 3.3 Structural model 10

4. RESULTS THERMAL ANALYSES 13

5. RESULTS STRUCTURAL ANALYSES 15
   - 5.1 Results for the surface breaking defect 15
   - 5.2 Results for the subclad defect 16

6. SUMMARY 19

REFERENCES 21

LIST OF SYMBOLS 23

FIGURES 25

1. INTRODUCTION

The main objective of NESC and particularly of the NESC1 spinning cylinder experiment as described in [1] are summarised below. NESC, the Network for the Evaluation of Steel Components, is the successor to the PISC network which was formally and successfully concluded in March 1994. PISC was principally concerned with inspection issues. NESC considers all aspects of the structural integrity assessment procedure and specifically the ways in which the inspection, fracture mechanics and material characterisation phases interact with one another to influence the overall assessment. The NESC launch project, NESC1, to be performed at the AEA laboratories Risley, UK, is a spinning cylinder experiment designed to address the cleavage initiation behaviour of both subclad and surface breaking defects in simulated end of life RPV material, exposed to a pressurised thermal shock transient.

The NESC1 spinning cylinder experiment will be performed on a forged cylinder of RPV material, clad with a thin stainless steel layer. A series of subclad and surface defects will be introduced to the cylinder. The cylinder will be circulated between the participating international organisations, who will perform non destructive examination (NDE) assessments of the cylinder with the objective of identifying and sizing the implanted defects. On completion of these assessments the PTS transient test will be performed. During this test the cylinder will be heated electrically to a uniform test temperature and rotated at a constant angular velocity. Upon stabilisation of the temperature and the rotational velocity , the inner cylinder is quenched by means of cold water spray jets to simulate the PTS transient. During the start-up and transient phases of the experiment surface temperatures, strains and defect initiation effects will be recorded by installed instrumentation.

The NESC Structural Analysis Task Group (TG3) has been charged with the performance of 3 specific tasks within the project:

- Pre-test analyses to assist the detailed design specification of the experiment and more specifically to advise on the range of defect sizes likely to lead to a cleavage initiation event.
- Defect assessments based on NDE defect definitions and idealised loading conditions.
- Defect assessments based upon the actual initial defect geometry and the actual experimental loading history and event data, to predict the extent of cleavage crack growth.

This report summarises the results of the pre-test structural analyses performed by the group Applied Mechanics at ECN - Nuclear Energy. The structural analyses have been performed for a forged cylinder with a 4 mm cladding and a semi elliptical defect with a depth of 40 mm and an aspect ratio of 1 : 3. The behaviour of both a spinning cylinder with a surface breaking and with a subclad defect are investigated with elastic as well as elasto-plastic three-dimensional finite element analyses.

2. GEOMETRY, MATERIAL PROPERTIES AND LOADING CONDITIONS

The group Applied Mechanics at ECN - Nuclear Energy has performed pre-test structural analyses for the spinning cylinder experiment. The structural analyses are performed for a cylinder with a semi elliptical defect with a depth of 40 mm and an aspect ratio (a : c) of 1 : 3. Both a surface breaking and a subclad defect are investigated. The behaviour of the spinning cylinder with a defect is investigated with an elastic as well as an elasto-plastic analysis.

2.1 Geometry description

The geometry of the cylinder with the defect is illustrated in figure 1. The principal dimensions of the geometry are [1]:

cylinder internal diameter	:	1150	mm
cylinder wall thickness (inclusive cladding)	:	150	mm
cylinder cladding thickness	:	4	mm
cylinder length	:	1300	mm
defect depth a	:	40	mm
half the defect width c	:	120	mm

2.2 Material properties

The spinning cylinder consists of a forged cylinder of a Reactor Pressure Vessel steel with an internal cladding. The cylinder is a forging of material *A508B*. The elastic, plastic and thermal material properties of *A508B* are [1]:

Young's modulus	E(0°C)	:	212350	N mm^{-2}
	E(350°C)	:	189100	N mm^{-2}
Poisson ratio	ν	:	0.28	
density	ρ	:	7787	kg m^{-3}
thermal conductivity	λ	:	33.92	W m^{-1} K^{-1}
specific heat	c_h	:	541	J kg^{-1} K^{-1}
coefficient of thermal expansion	α(0°C)	:	1.186E-05	K^{-1}
	α(350°C)	:	1.340E-05	K^{-1}
yield stress	σ_y	:	510	N mm^{-2}

The cladding consists of the material *308/9 SS*. The elastic, plastic and thermal material properties for the cladding material are [1]:

Young's modulus	E(20°C)	:	200000	N mm^{-2}
	E(288°C)	:	178000	N mm^{-2}
Poisson ratio	ν	:	0.30	
density	ρ	:	7920	kg m^{-3}
thermal conductivity	λ	:	15.30	W m^{-1} K^{-1}
specific heat	c_h	:	495	J kg^{-1} K^{-1}

coefficient of thermal expansion	$\alpha_{(20°C)}$	:	1.389E-05	K^{-1}
	$\alpha_{(288°C)}$	:	1.850E-05	K^{-1}
yield stress	σ_y	:	210	N mm^{-2}

For both materials the Young's modulus and the coefficient of thermal expansion are temperature dependent. It is assumed that these properties vary linear with the temperature. In the elasto-plastic analyses the work hardening of both materials is ignored, an elastic, perfectly plastic material behaviour is assumed.

2.3 Loading conditions

During the experiment the cylinder is subjected to a thermal and a mechanical load by which a pressurised thermal shock in a reactor pressure vessel is simulated. The pressure load is simulated by rotating the cylinder. For the current analyses a constant rotational velocity of 2500 rpm is assumed. The thermal shock conditions are simulated by the injection of cold water of 5°C at the inside of the cylinder which has been heated to a uniform temperature of 315°C. The rate at which the accumulated heat is drained from the cylinder is determined by the temperature difference between the water and the inside cylinder surface and the heat transfer coefficient. For the structural analysis it is assumed that the cylinder is in a stress free state at 315°C. Summarising the *loading conditions* used for the analyses performed by ECN:

initial cylinder temperature	:	315	°C
water injection temperature	:	5	°C
rotational velocity	:	2500	rpm
heat transfer coefficient during quench	:	22	kW m^{-2} K^{-1}
stress free temperature	:	315	°C

3. MODEL DESCRIPTION

The behaviour of the spinning cylinder due to the thermal and mechanical loads representing a pressurised thermal shock condition is determined by means of finite element calculations. Two separate calculations are made. The time-dependent temperature distribution is determined with a thermal transient analysis. To determine the thermo-mechanical behaviour of the spinning cylinder both elastic and elasto-plastic fracture mechanics analyses are performed. For the surface breaking defect and the subclad defect the combinations of performed finite element analyses are summarised in table 1. Two thermal transient analyses and four structural analyses are performed. Although the temperature distributions for all four analyses are identical two thermal transient analyses had to be made, because the used mesh layouts for the elastic and the elasto-plastic analyses are not exactly the same in the crack tip elements.

Table 1 *The combinations of finite element analyses, which are performed*

the spinning cylinder with the surface breaking defect		the spinning cylinder with the subclad defect	
thermal transient analysis 1	thermal transient analysis 2	thermal transient analysis 1	thermal transient analysis 2
elastic structural analysis 1	elasto-plastic structural analysis 1	elastic structural analysis 2	elasto-plastic structural analysis 2

3.1 Mesh layout

All the analyses summarised in table 1 are three-dimensional finite element calculations. For the corresponding thermal transient analysis and structural analysis the same mesh layout is used. Figure 2 shows the applied mesh layout for the spinning cylinder. This mesh layout is made with the pre-processor of the general purpose finite element program ANSYS 5.0a [2]. Due to the symmetry of the geometry with respect to the *xy*- and *xz*-plane only a quarter of the spinning cylinder had to be modelled. The mesh consists of 1412 20-node hexahedral elements and 7177 nodal points. Figure 3 shows the mesh layout near the defect. The crack front is modelled with 72 20-node hexahedral elements collapsed to wedges.

3.2 Thermal transient model

The thermal transient analyses determine the temperature distribution in the spinning cylinder as a function of time. The thermal transient analyses are performed with the general purpose finite element program MARC K6.1 [3]. For the thermal transient analyses the mesh consists of MARC type 44 elements. MARC element type 44 is a three-dimensional 20-node heat transfer brick element with triquadratic interpolation functions for an accurate

representation of the temperature field.

It is assumed that there is no heat flow through the outside surfaces of the model, with the exception of the inside cladding surface. For these surfaces an insulated boundary condition is specified. At the inside cladding surface the quench with the cold water is simulated with the FILMS option [3]. With this option the appropriate heat transfer coefficient and associated water temperature (sink temperature) are specified.

The defect has no influence on the distribution of the temperature field in the spinning cylinder. Consequently for the spinning cylinder with the surface breaking defect and the spinning cylinder with the subclad defect no separate thermal transient analyses have to be performed. The material properties (thermal conductivity, density and specific heat) and the loading conditions (initial temperature, sink temperature and heat transfer coefficient) for the thermal transient analyses are taken as specified in the previous chapter.

A thermal transient analysis is an incremental calculation. For the analyses performed for the spinning cylinder the temperature change in an increment was limited to 15 K.

3.3 Structural model

The structural analyses are fracture mechanics analyses to determine the crack driving force. The structural analyses are performed with the general purpose finite element program MARC K6.1 [3]. For the structural analyses the mesh consists of MARC type 21 elements. MARC element type 21 is a three-dimensional 20-node isoparametric element. The element uses triquadratic interpolation functions to represent the coordinates and displacements, which allows for an accurate representation of the strain field [3].

For the elastic fracture mechanics analyses the hexahedral elements used to model the crack front are collapsed to wedges as illustrated in figure 4. The element midside nodes next to the crack front (nodes 9, 11, 13 and 15 in figure 4) have a quarter point position. The coinciding nodes on the crack front are tied in all directions. In this way it is ensured that the elements collapsed to wedges show the correct singularity ($r^{-½}$) in the strain field for elastic fracture mechanics analyses [4].

For the elasto-plastic fracture mechanics analyses the hexahedral elements used to model the crack front are collapsed to wedges as illustrated in figure 5. The element midside nodes (nodes 9, 11, 13 and 15 in figure 5) are situated at the middle of the element side. The coinciding nodes on the crack front are not tied. The material behaviour is assumed to be elastic, perfectly plastic. In this way it is ensured that the elements collapsed to wedges show the correct singularity (r^{-1}) in the strain field for elasto-plastic fracture mechanics analyses [4].

The boundary conditions for the structural model are applied to the symmetry surfaces. On the xy-surface the z-displacement is suppressed. On the xz-surface the y-displacement is suppressed with the exception of the defect area. The surface breaking defect and the subclad defect are modelled by applying the correct symmetry boundary conditions for the cladding at the defect. For the surface breaking defect the y-displacements of the cladding in the defect area are not suppressed, while for the subclad defect the y-displacements are suppressed. The centrifugal load is specified with the option ROTATION A [3]. The thermal loads as determined with the thermal

transient analysis are applied with the option TRANSIENT [3].

For the structural analyses the material properties (Young's modulus, Poisson ratio, density and coefficient of thermal coefficient) and the centrifugal load are taken as specified in chapter 2. For the elasto-plastic structural analyses also the yield stresses given in chapter 2 are specified.

For the extraction of the fracture mechanics parameters J and K_J from the results of the finite element structural analyses the MARC program offers the LORENZI option, which is specially suited for problems which incorporate plastic deformations and thermal loadings [3]. In a number of locations (figure 6) along the crack front, which coincide with the corner nodes of the wedged crack tip elements, the LORENZI option determines the variation in the strain energy ΔE using the virtual crack extension method [3, 4]. The variation in the strain energy ΔE is divided by the change in crack surface area Δa to obtain the J-integral:

$$J = \frac{2 \cdot \Delta E}{\Delta a}$$

The stress intensity factor K_J is determined from the J-integral with the following relation:

$$K_J = \sqrt{\frac{E}{1-\nu^2} \cdot J}$$

where:

E : Young's modulus (temperature dependent)
J : J-integral
K_J : stress intensity factor derived from the J-integral
ν : Poisson ratio

4. RESULTS THERMAL ANALYSES

As already mentioned the thermal transient analyses have been performed with the use of the general purpose finite element program MARC K6.1 [3]. The mesh layout for the elastic and the elasto-plastic analyses is identical with the exception of the position of the midside nodes in the crack tip elements. This has no influence on the thermal behaviour of the spinning cylinder. It only influences the determined nodal temperatures, which are used as input for the structural analyses. In this chapter the determined overall thermal behaviour of the spinning cylinder is discussed.

Initially the spinning cylinder has a uniform temperature of 315°C. At time t = 0 s the quench of the inside cladding surface is started. In the figures 7 to 10 the temperature distribution in the spinning cylinder is shown after respectively 1, 300, 600 and 900 seconds. Due to the quench of the inside cladding surface with cold water a temperature gradient through the wall thickness is introduced. The isothermal surfaces are parallel to the cylinder surfaces and move as the quench lasts from the inside to the outside of the cylinder. In the first moments the introduced temperature gradient is very sharp.

Figure 11 shows the temperature at the inside and the outside of the cylinder as a function of time. At the inside of the spinning cylinder the temperature decreases very rapidly, while at the outside the temperature decreases slowly. For various points in time the temperature gradient through the wall thickness is shown in figure 12. This figure illustrates that the temperature gradient initially is very sharp and levels off as time increases.

For the locations along the crack front (depicted in figure 6) the temperature as a function of time is shown in figure 13. Figure 14 shows the temperature distribution along the crack front as a function of the *s*-coordinate (figure 6) for various points in time.

The determined thermal transient results (element temperatures) are fed into the structural analyses to calculate the thermal strains.

5. RESULTS STRUCTURAL ANALYSES

The structural analyses are performed as already mentioned with the general purpose finite element program MARC K6.1 [3]. The development of the stresses and strains in the spinning cylinder is influenced by the geometry of the defect and the loading. The loading of the spinning cylinder is a combination of a constant centrifugal load and a varying thermal load due to the temperature gradient, the temperature dependent material behaviour and the difference in thermal expansion between the vessel and the cladding. With the structural analyses the distribution of the stresses and strains in the spinning cylinder is determined as a function of time. For the defect the fracture mechanics parameters J and K_J are determined also. The results for the spinning cylinder with the surface breaking defect are presented in section 5.1. The results for the spinning cylinder with the subclad defect are presented in section 5.2.

5.1 Results for the surface breaking defect

The figures 15 and 16 show the distribution of the equivalent von Mises stress through the wall thickness at the location where the defect depth is maximal for 0, 300 and 600 seconds. Figure 15 shows the distribution of the equivalent stress determined with the elastic structural analysis, while the distribution determined with the elasto-plastic structural analysis is shown in figure 16. These figures illustrate the stress peak to be found at the crack tip. In figure 16 the stress peak at the crack tip is limited by the yield stress of the cylinder.

The distribution of the circumferential stress through the wall thickness at the location where the defect depth is maximal is shown in the figures 17 and 18, respectively for the elastic and the elasto-plastic structural analysis. The circumferential stress is the stress component perpendicular to the defect plane. These figures show that the defect area is stress free in circumferential direction. Peak stresses arise at the crack tip. Initially only tensile circumferential stresses are found through the wall thickness due to the centrifugal load. Due to the quench at the inside of the cylinder compressive circumferential stresses develop at the outside of the cylinder.

Figure 19 shows the development in time of the J-integral as determined with the elastic structural analysis at the locations along the crack front depicted in figure 6. The development of the J-integral as determined with the elasto-plastic structural analysis is shown in figure 20. The elasto-plastic structural analysis is stopped after 600 seconds due to numerical problems. These numerical problems are caused by the closing of the defect in the cladding due to plastic deformations. It is observed that the defect area has penetrated the plane of symmetry (xz-plane). In future analyses this could be solved by the introduction of gap elements at the defect area.

Figure 21 and 22 show the J-integral as a function of temperature at various locations along the crack front for respectively the elastic and the elasto-plastic structural analysis. The J-integral along the crack front is shown in figure 23 as determined with the elastic structural analysis and in figure 24 as determined with the elasto-plastic structural analysis. The results shown in figure 24 for 600 seconds should be regarded with caution due to the, above

mentioned, encountered numerical problems.

With the J-integral the stress intensity factor K_J is determined. The stress intensity factor K_J determined with the elastic structural analysis is shown in the figures 25, 27 and 29. The figures 26, 28 and 30 show the stress intensity factor K_J determined with the elasto-plastic structural analysis. The stress intensity factor K_J is shown as a function of time in figure 25 and 26 for various locations along the crack front. For the same locations the development of the stress intensity factor K_J is shown in figure 27 and 28 as a function of temperature. For various points in time the stress intensity factor K_J along the crack front is shown in figure 29 and 30.

With the elastic and the elasto-plastic structural analysis different stress intensity factors K_J are obtained. For the locations 1 and 8 depicted in figure 6 this is illustrated in figure 31. This figure shows for both locations the stress intensity factors K_J as a function of temperature as determined with the elastic as well as with the elasto-plastic structural analysis. The elastic structural analysis predicts higher stress intensity factors K_J than the elasto-plastic structural analysis.

5.2 Results for the subclad defect

The distribution of the equivalent von Mises stress through the wall thickness at the location where the defect depth is maximal is shown in figure 32 and 33. Figure 32 shows the distribution of the equivalent stress at the points in time 0, 300 and 600 seconds as determined with the elastic structural analysis. The distribution determined with the elasto-plastic structural analysis is shown in figure 33. At the crack tip and in the cladding peak stresses are found. In the elasto-plastic structural analysis these peak stresses are limited to the yield stress of the vessel material or the cladding.

Figures 34 and 35 show the distribution of the circumferential stress through the wall thickness at the location where the defect depth is maximal. The distribution determined with the elastic structural analysis is shown in figure 34 and the distribution determined with the elasto-plastic structural analysis is shown in figure 35. Peak stresses arise in the cladding and at the crack tip. Due to the coarse mesh at the cladding-defect interface the defect area is not entirely stress free as should be expected.

The development and distribution of the J-integral as determined with the elastic structural analysis are shown in the figures 36, 38 and 40. Figure 36 shows the J-integral as a function of time at some locations along the crack front depicted in figure 6. For the same locations figure 38 shows the J-integral as a function of temperature. The distribution of the J-integral along the crack front at various points in time is shown in figure 40. In the figures 37, 39 and 41 the development and distribution of the J-integral determined with the elasto-plastic analysis is shown. For both the analyses the J-integral determined at end of the crack front at the cladding-cylinder interface (location 9 in figure 6) should be regarded with caution. For this location the direction of the crack front is ambiguous, which hampers the calculation of the strain energy variations with the LORENZI option.

The stress intensity factor K_J is determined from the J-integral. For the spinning cylinder with the subclad defect the figures 42, 44 and 46 show the

development and distribution of the stress intensity factor K_J as determined with the elastic structural analysis. The figures 43, 45 and 47 show the stress intensity factor K_J as determined with the elasto-plastic analysis. Figure 42 and 43 show the stress intensity factor K_J as a function of time. The stress intensity factor K_J as a function of temperature is shown in the figures 44 and 45. The distribution of the stress intensity factor K_J along the crack front at various time intervals is shown in figure 46 and 47.

With the elastic and the elasto-plastic structural analysis different stress intensity factors K_J are obtained. This is illustrated in figure 48 for the locations 1 and 8 along the crack front depicted in figure 6. For these locations figure 48 shows the stress intensity factors K_J as a function of temperature determined with the elastic as well as the elasto-plastic structural analysis. The elasto-plastic structural analysis predicts distinct higher stress intensity factors K_J than the elastic structural analysis. The stress intensity factors K_J predicted for the subclad defect (figure 48) are lower than the stress intensity factors predicted for the surface breaking defect (figure 31).

6. SUMMARY

The group Applied Mechanics at ECN - Nuclear Energy performed pre-test structural analyses for the NESC1 spinning cylinder experiment. The crack driving force for a forged cylinder with a 4 mm cladding and a semi elliptical defect with a depth of 40 mm and an aspect ratio of 1 : 3 is determined with three-dimensional finite element calculations. With thermal transient analyses the influence of the experimentally applied thermal shock on the cylinder is determined. With elastic and elasto-plastic fracture mechanics analyses the crack driving force for a spinning cylinder with a surface breaking defect as well as a spinning cylinder with a subclad defect is determined. For the defects the fracture mechanics parameters J and K_J are computed.

With the performed structural analyses different results are obtained for the spinning cylinder with the surface breaking defect and the spinning cylinder with the subclad defect. For the surface breaking defect the elastic structural analysis predicted slightly higher stress intensity factors than the elasto-plastic structural analysis (figure 31). While for the subclad defect the elasto-plastic structural analysis predicted distinct higher stress intensity factors than the elastic structural analysis (figure 48). The stress intensity factors determined for the surface breaking defect are higher than the stress intensity factors determined for the subclad defect. The differences in the predicted stress intensity factors between the surface breaking and the subclad defect are substantial according to the elastic structural analyses and small according to the elasto-plastic structural analyses.

REFERENCES

[1] S. McAllister, S. Bhandari: *NESC spinning cylinder experiment: pre-test structural analysis evaluation.*

[2] Swanson Analysis Systems, Inc: *ANSYS User's Manuals.* Revision 5.0a, (1992).

[3] MARC Analysis Research Corporation: *MARC User's Manuals.* Revision K6.1, (1994).

[4] J. Prij: *Investigations on crack growth parameters in the elastic plastic region.* Netherlands Energy Research Foundation ECN, ECN-114, March 1982.

LIST OF SYMBOLS

a	defect depth	[m]
Δa	change in the crack surface area	[m^2]
c	half the defect width	[m]
c_h	specific heat	[J kg^{-1} K^{-1}]
E	Young's modulus	[N m^{-2}]
ΔE	variation in the strain energy	[J]
h	heat transfer coefficient	[W m^{-2} K^{-1}]
J	J-integral	[N m^{-1}]
K_J	stress intensity factor derived from the J-integral	[MPa $m^{-0.5}$]
α	linear coefficient of thermal expansion	[K^{-1}]
λ	thermal conductivity	[W m^{-1} K^{-1}]
ν	Poisson ratio	
ρ	density	[kg m^{-3}]
σ_y	yield stress	[N m^{-2}]

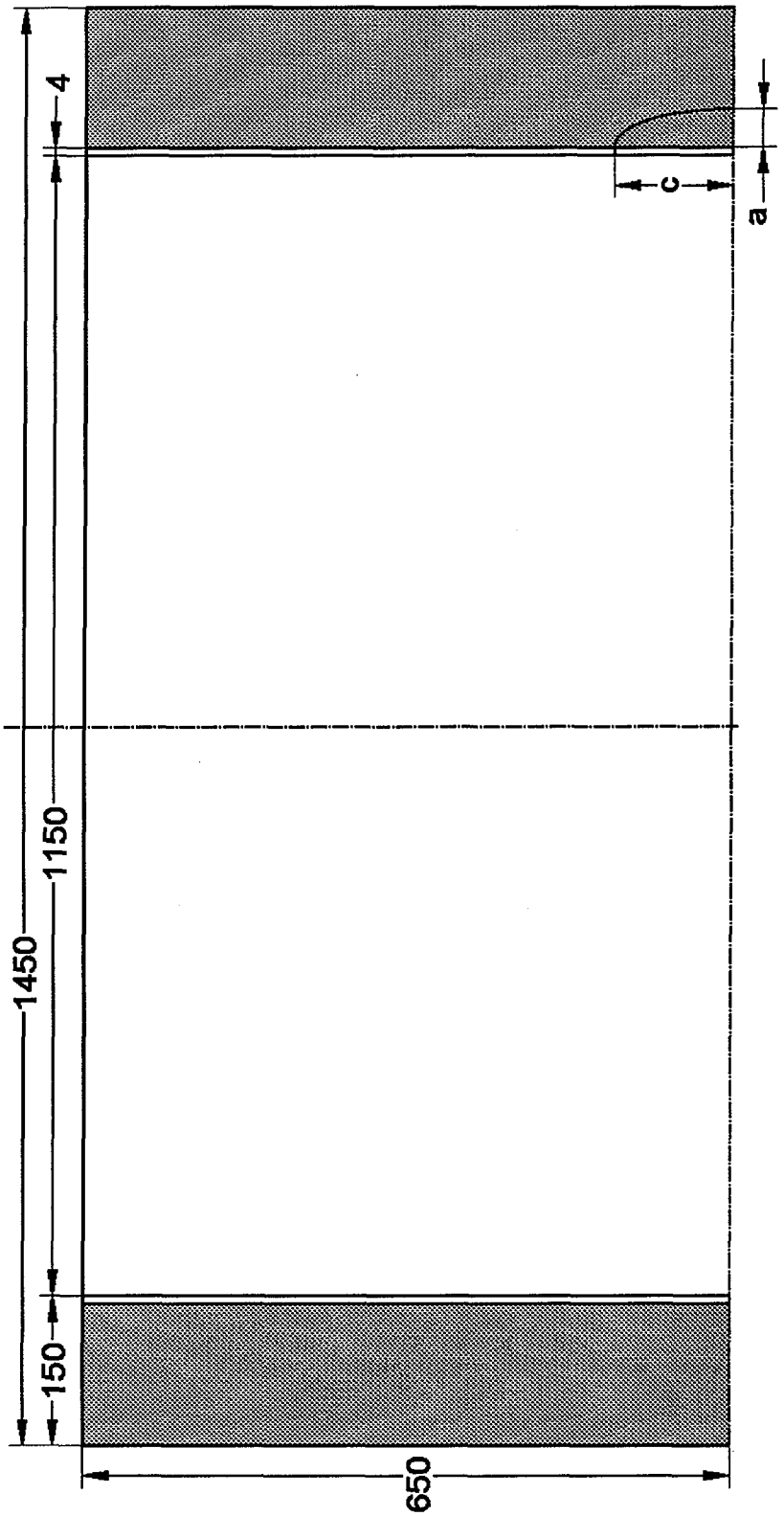

Figure 1 *Half the geometry of the NESC1 spinning cylinder with the semi elliptical defect*

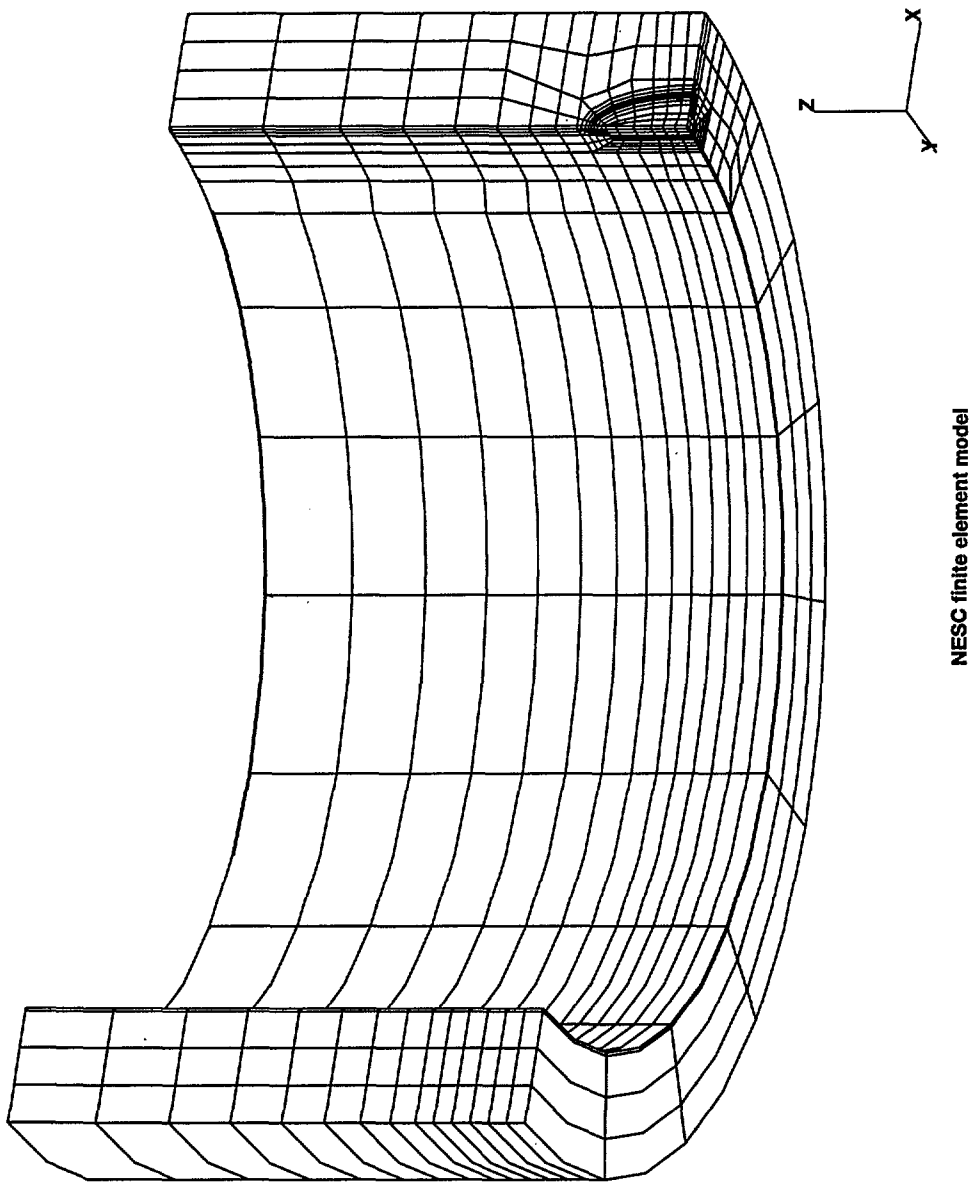

Figure 2 *NESC1 spinning cylinder*
Mesh layout for the elastic and elasto-plastic analyses

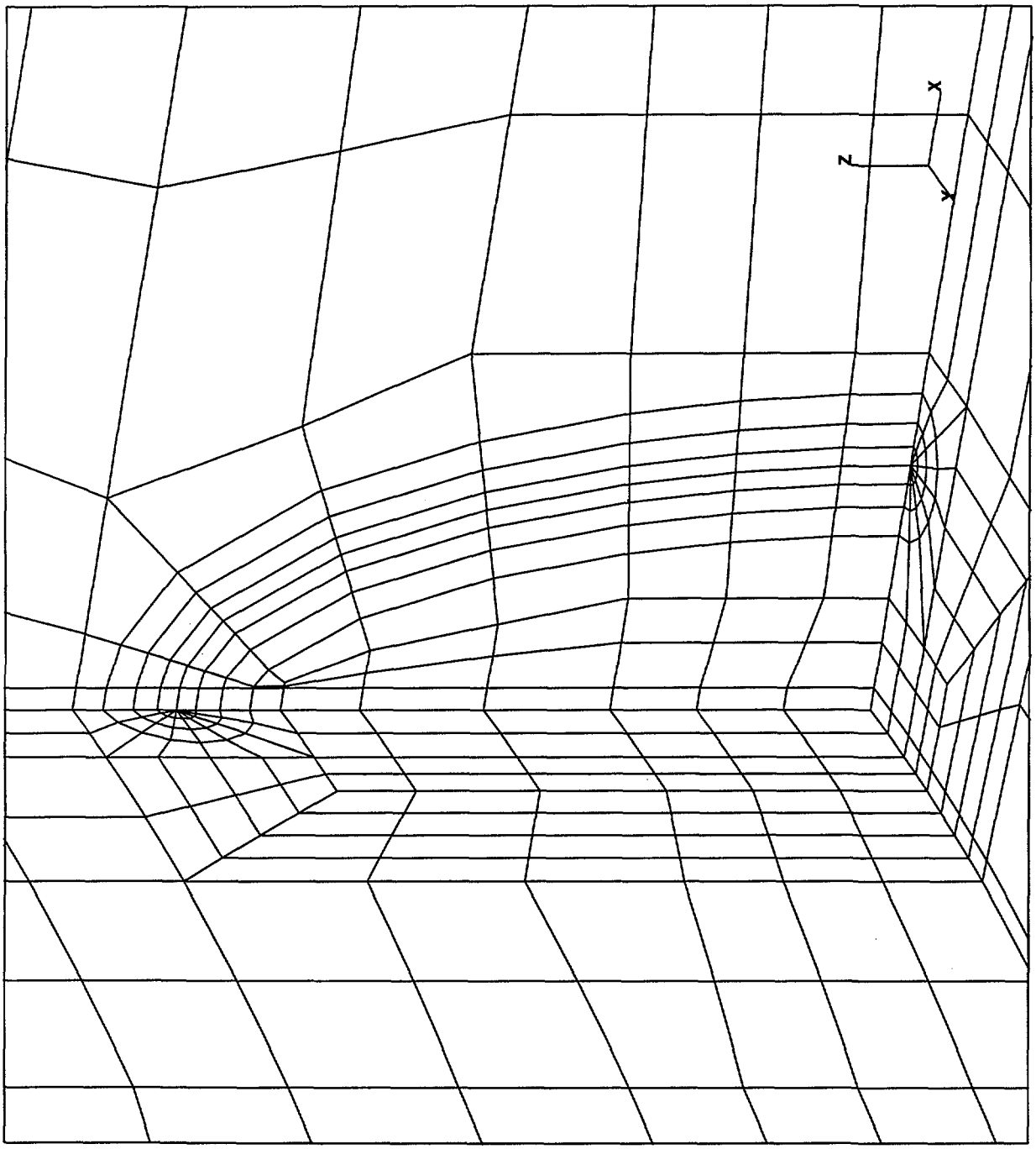

Figure 3 *NESC1 spinning cylinder*
Mesh layout at the semi elliptical defect for the elastic and eleasto-plastic analyses

$x_1 = x_{12} = x_4$

$x_{17} = x_{20}$

$x_5 = x_{16} = x_8$

$x_9 = \frac{1}{4}\,(x_2 + 3x_1)$

$x_{11} = \frac{1}{4}\,(x_3 + 3x_4)$

$x_{13} = \frac{1}{4}\,(x_6 + 3x_5)$

$x_{15} = \frac{1}{4}\,(x_7 + 3x_8)$

$x_{10} = \frac{1}{2}\,(x_2 + x_3)$

$x_{14} = \frac{1}{2}\,(x_6 + x_7)$

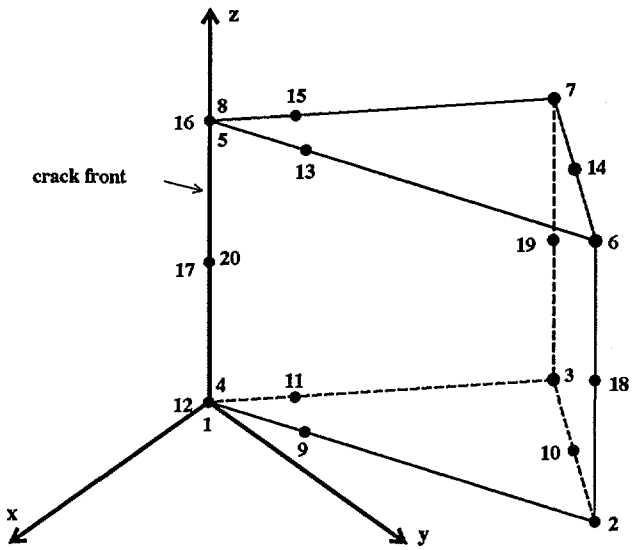

y and z analogously

Figure 4 *The collapsed 20-node brick element for an elastic fracture mechanics analysis*

$x_1 = x_{12} = x_4$

$x_{17} = x_{20}$

$x_5 = x_{16} = x_8$

$x_9 = \frac{1}{2}\,(x_2 + x_1)$

$x_{11} = \frac{1}{2}\,(x_3 + x_4)$

$x_{13} = \frac{1}{2}\,(x_6 + x_5)$

$x_{15} = \frac{1}{2}\,(x_7 + x_8)$

$x_{10} = \frac{1}{2}\,(x_2 + x_3)$

$x_{14} = \frac{1}{2}\,(x_6 + x_7)$

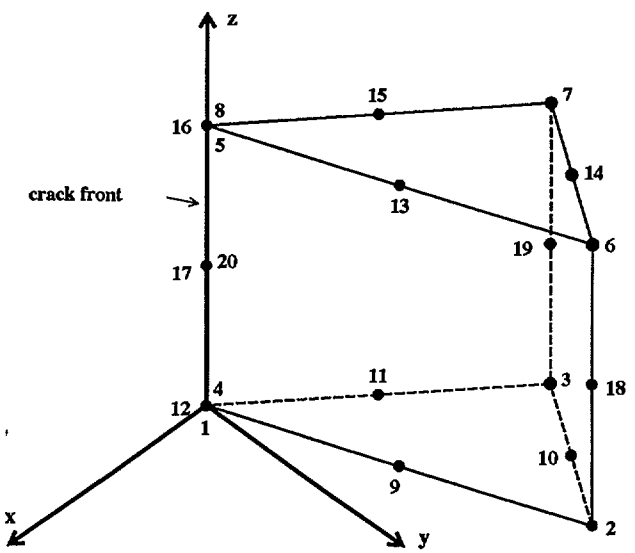

y and z analogously

Figure 5 *The collapsed 20-node brick element for an elasto-plastic fracture mechanics analysis*

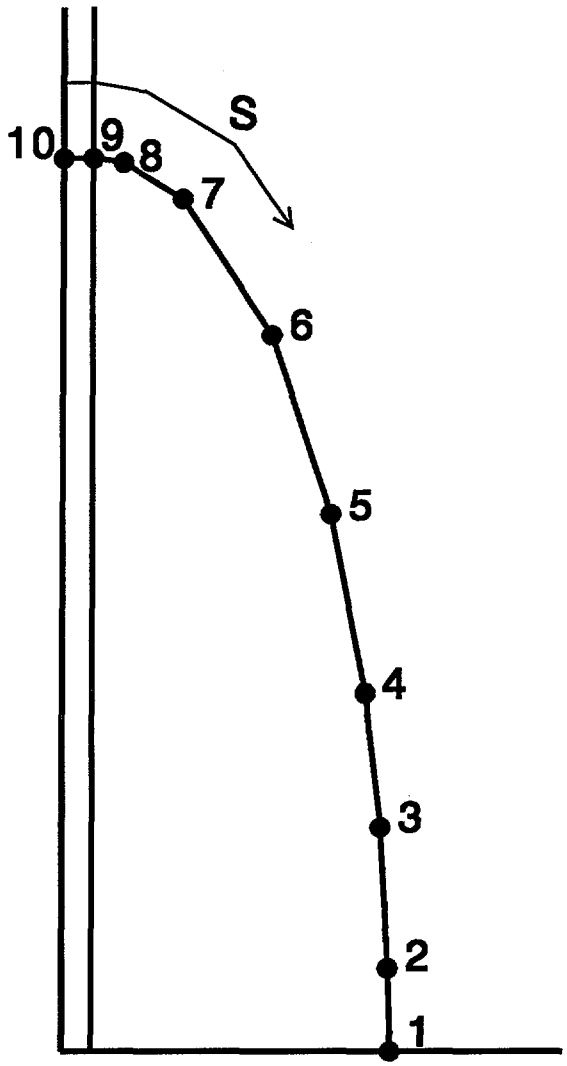

Figure 6 *The position of locations along the crack front where the fracture mechanics parameters are determined*

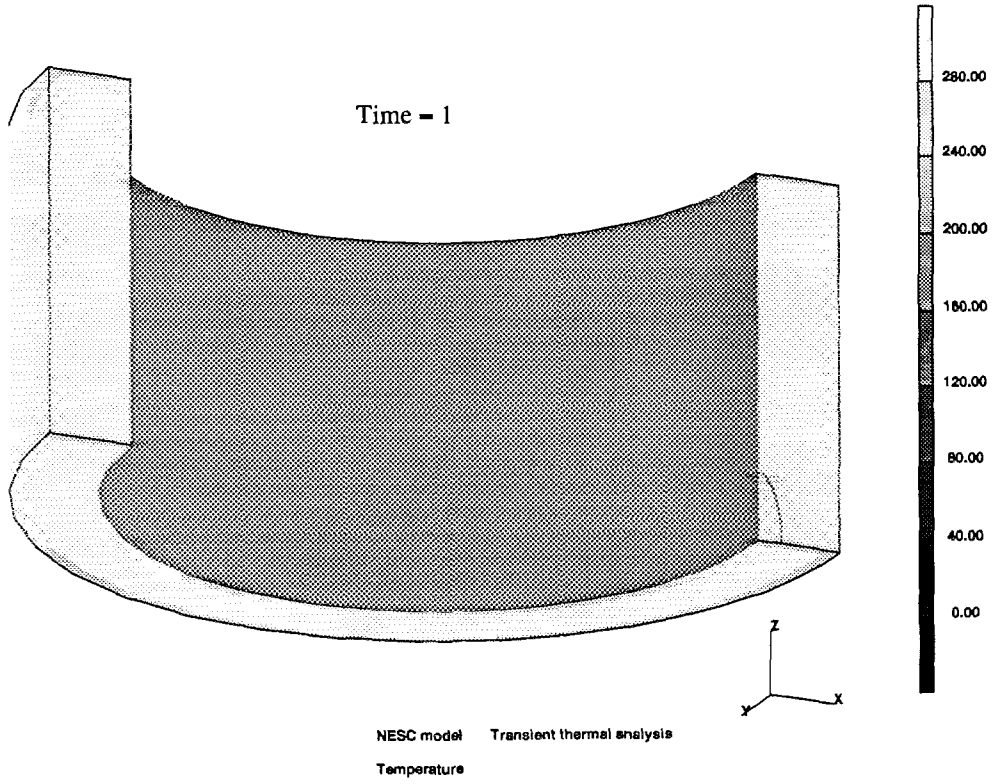

Figure 7 *The thermal transient analysis*
The temperature distribution at t = 1 sec

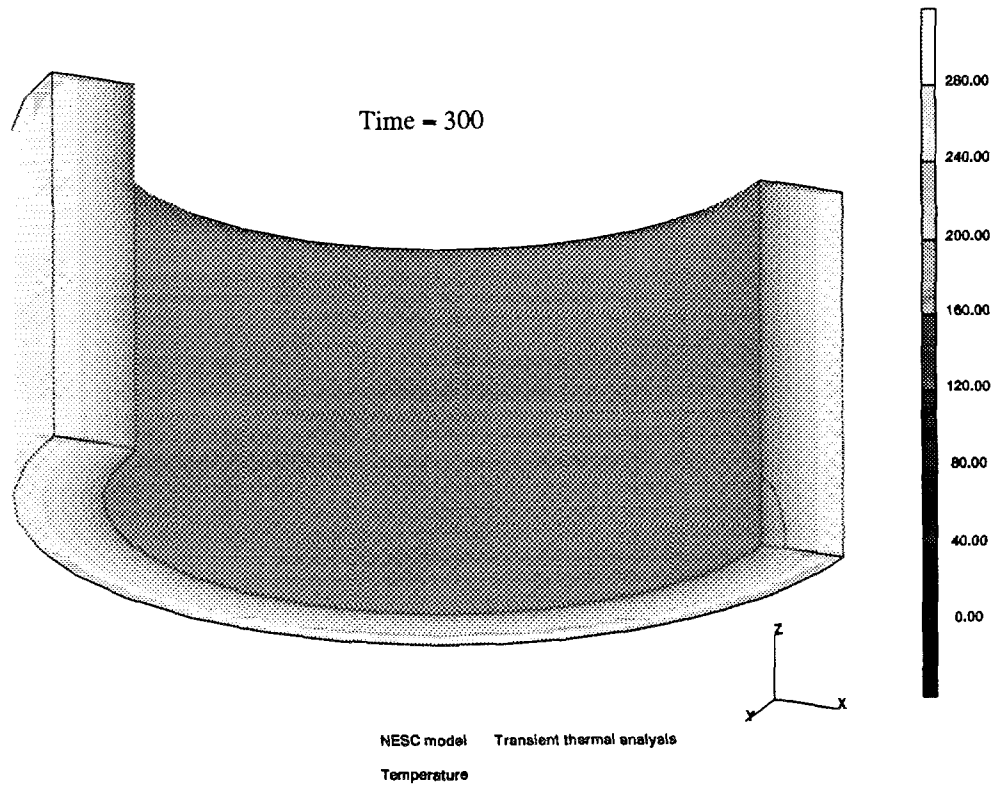

Figure 8 *The thermal transient analysis*
The temperature distribution at t = 300 sec

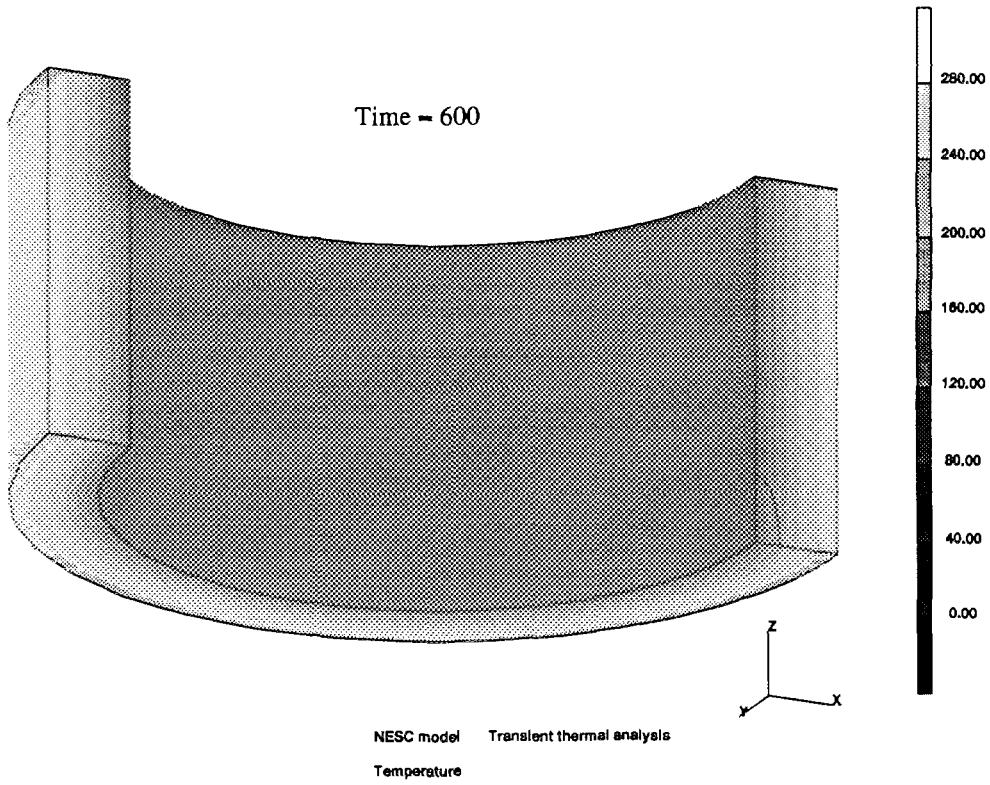

Figure 9 *The thermal transient analysis*
The temperature distribution at t = 600 sec

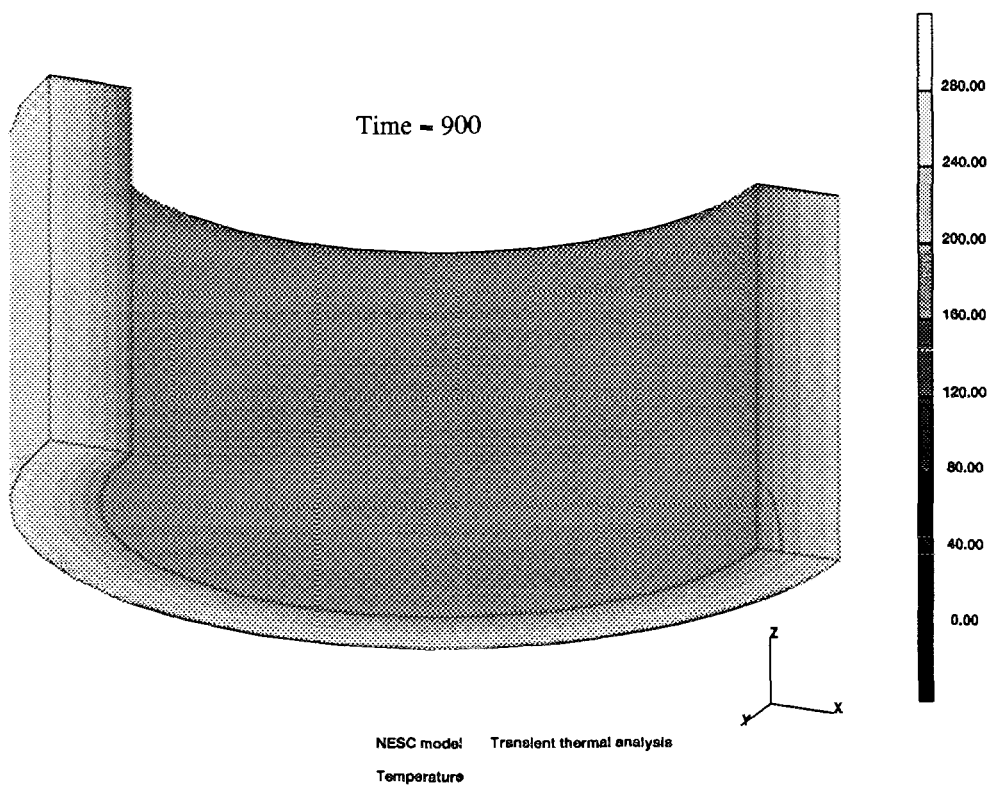

Figure 10 *The thermal transient analysis*
The temperature distribution at t = 900 sec

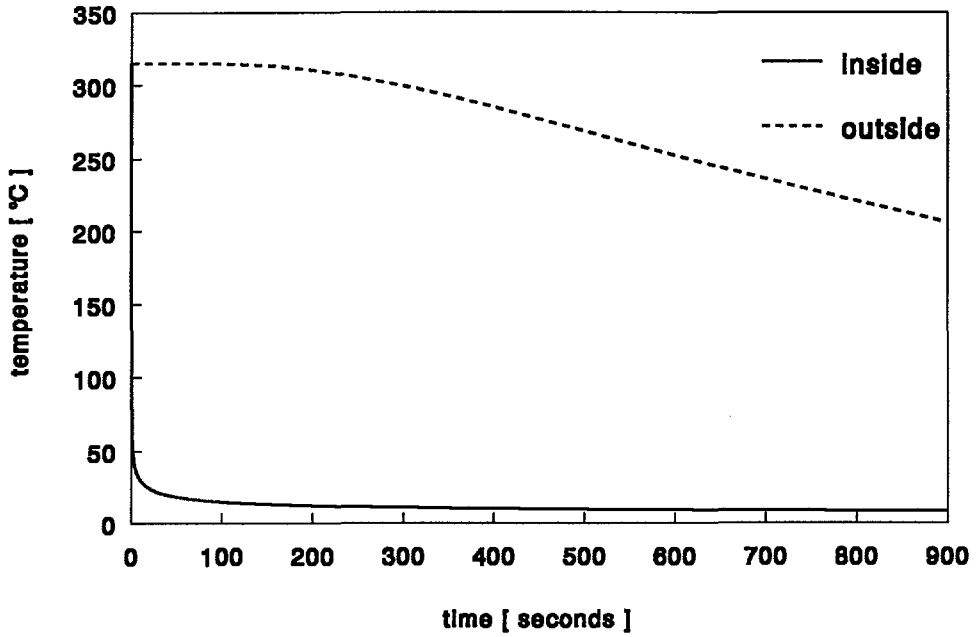

Figure 11 *The thermal transient analysis*
The temperature at the inside and the outside of the spinning cylinder as a function of time

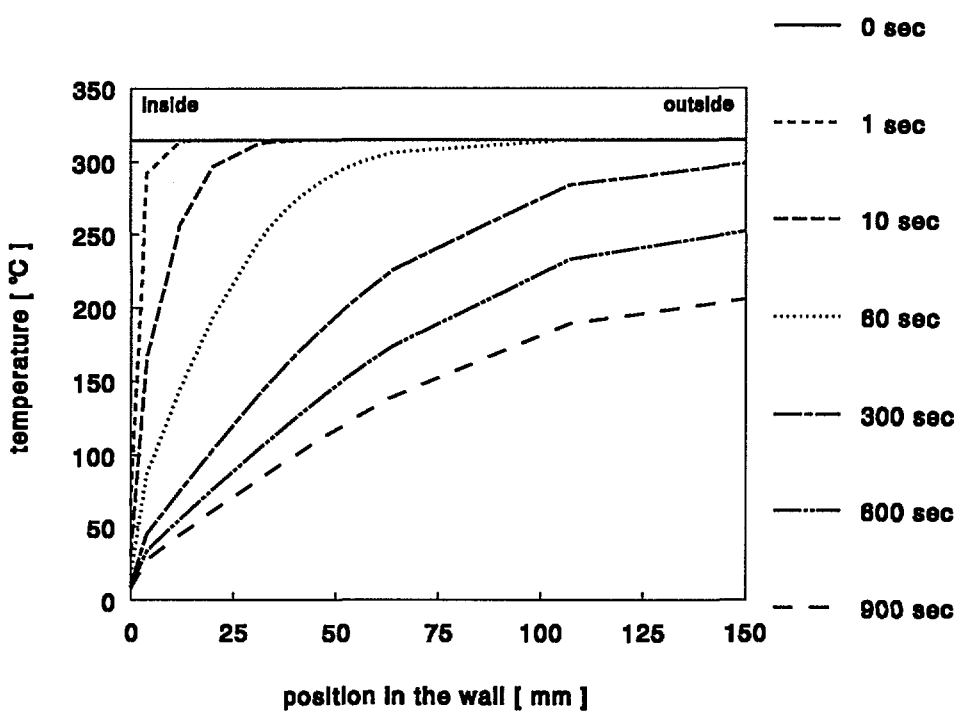

Figure 12 *The thermal transient analysis*
The temperature gradient through the wall thickness at various points in time

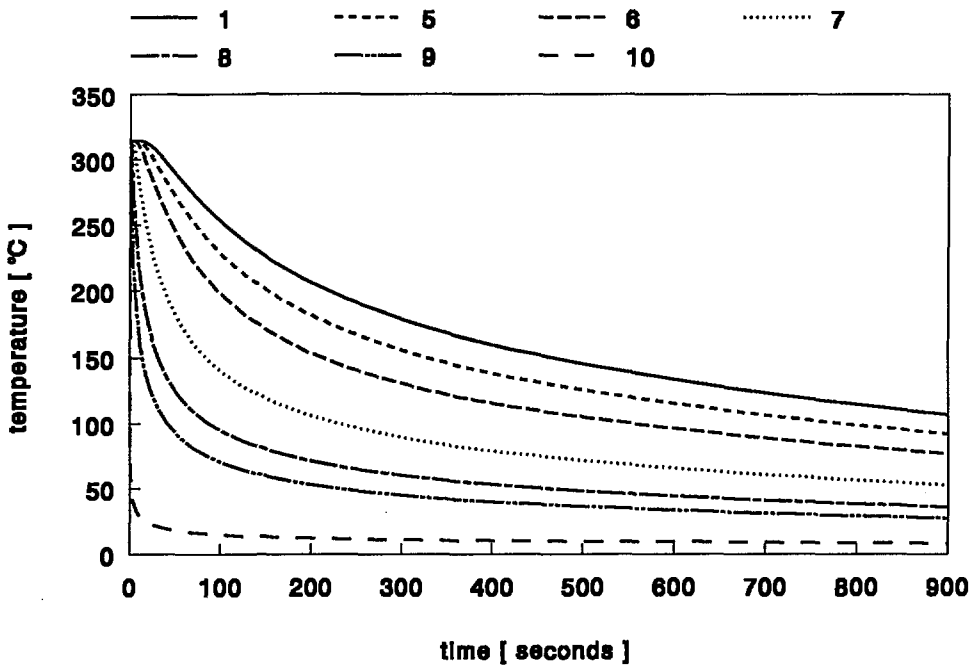

Figure 13 *The thermal transient analysis*
The temperature as a function of time in various locations along the crack front depicted in figure 6

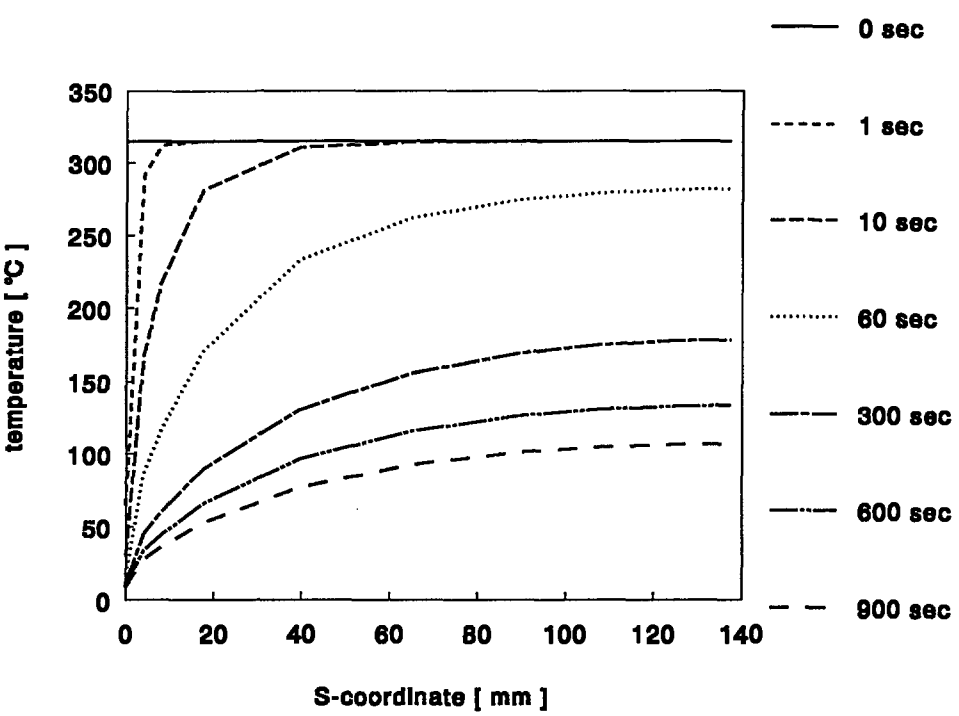

Figure 14 *The thermal transient analysis*
The temperature distribution along the crack front at various points in time

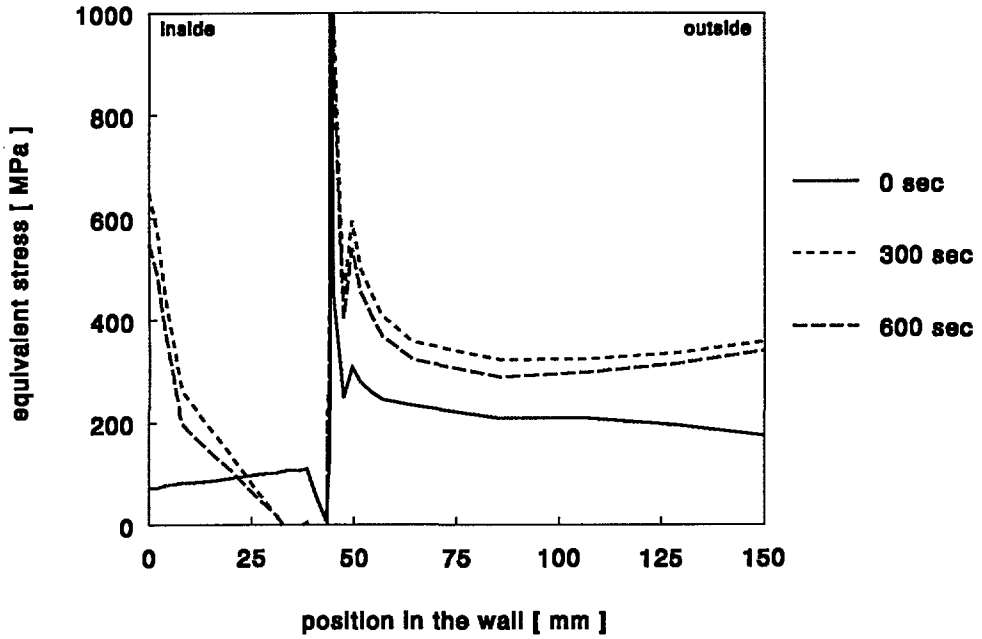

Figure 15 *The spinning cylinder with the surface breaking defect*
The equivalent stress through the wall thickness for various points in time as determined with the elastic structural analysis

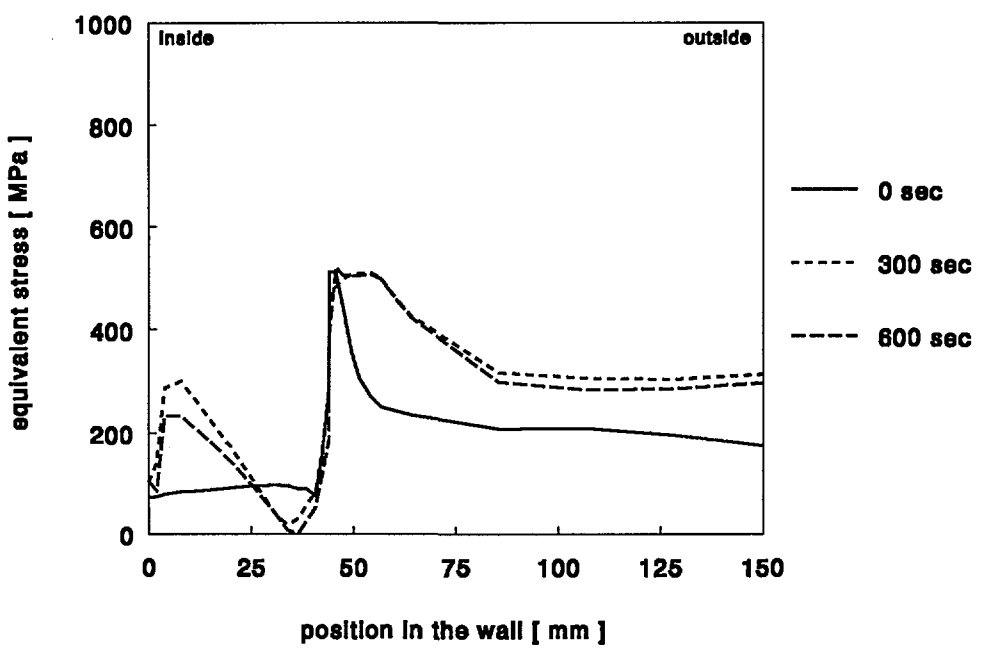

Figure 16 *The spinning cylinder with the surface breaking defect*
The equivalent stress through the wall thickness for various points in time as determined with the elasto-plastic structural analysis

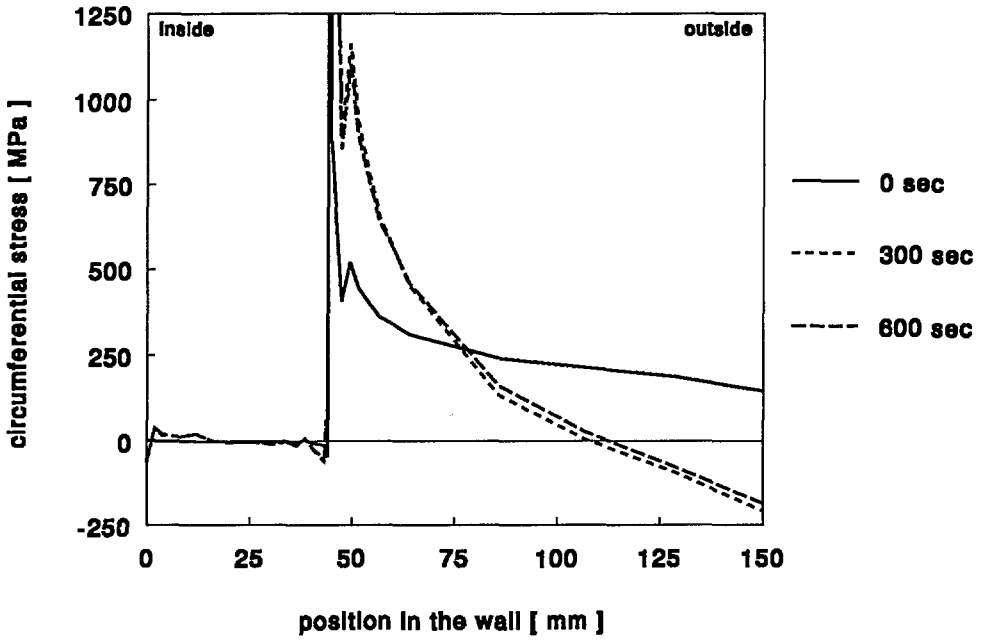

Figure 17 *The spinning cylinder with the surface breaking defect*
The circumferential stress through the wall thickness for various points in time as determined with the elastic structural analysis

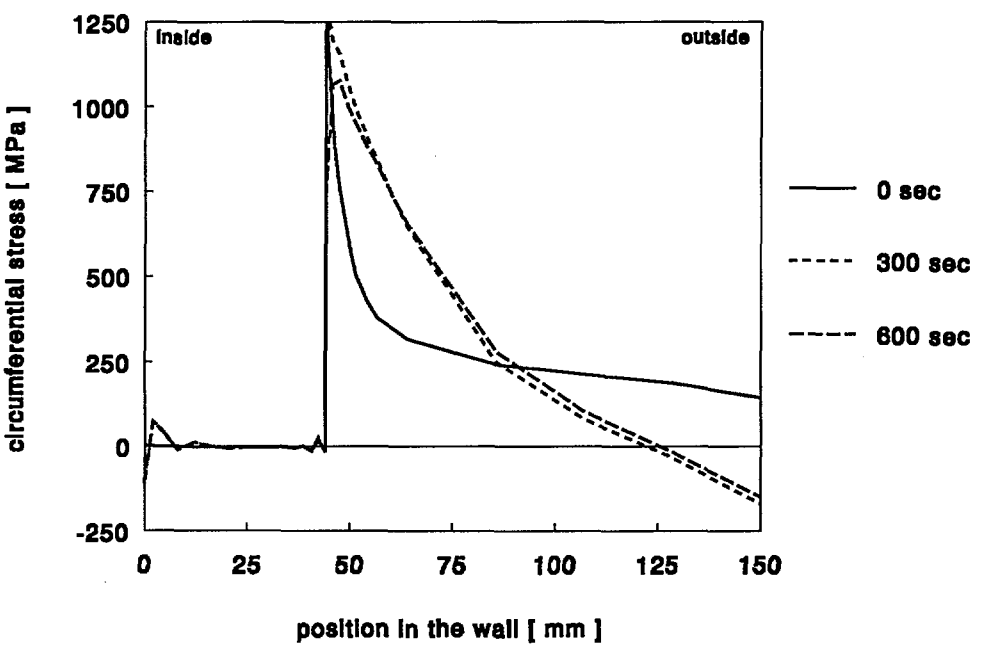

Figure 18 *The spinning cylinder with the surface breaking defect*
The circumferential stress through the wall thickness for various points in time as determined with the elasto-plastic structural analysis

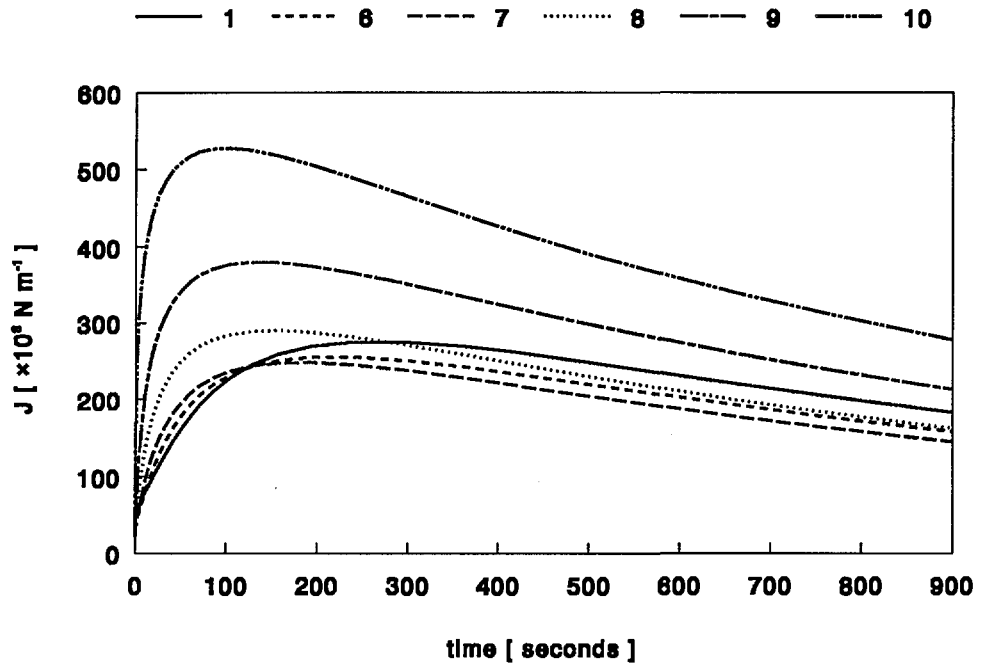

Figure 19 *The spinning cylinder with the surface breaking defect*
The J-integral as a function of time for some locations along the crack front (fig. 6) as determined with the elastic structural analysis

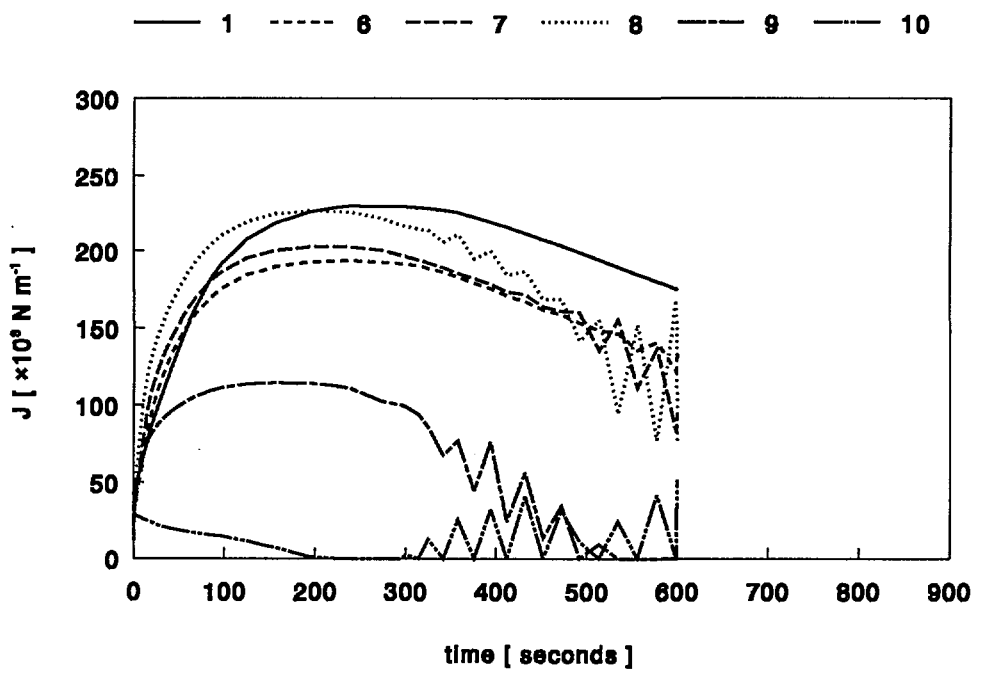

Figure 20 *The spinning cylinder with the surface breaking defect*
The J-integral as a function of time for some locations along the crack front (fig. 6) as determined with the elasto-plastic structural analysis

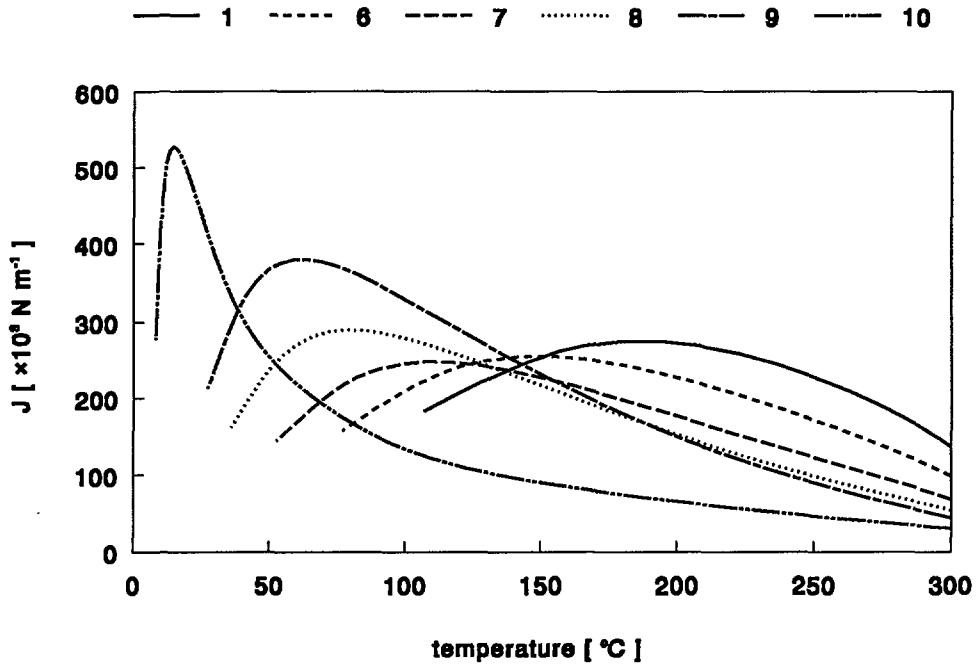

Figure 21 *The spinning cylinder with the surface breaking defect*
The J-integral as a function of temperature for some locations along the crack front (fig. 6) as determined with the elastic structural analysis

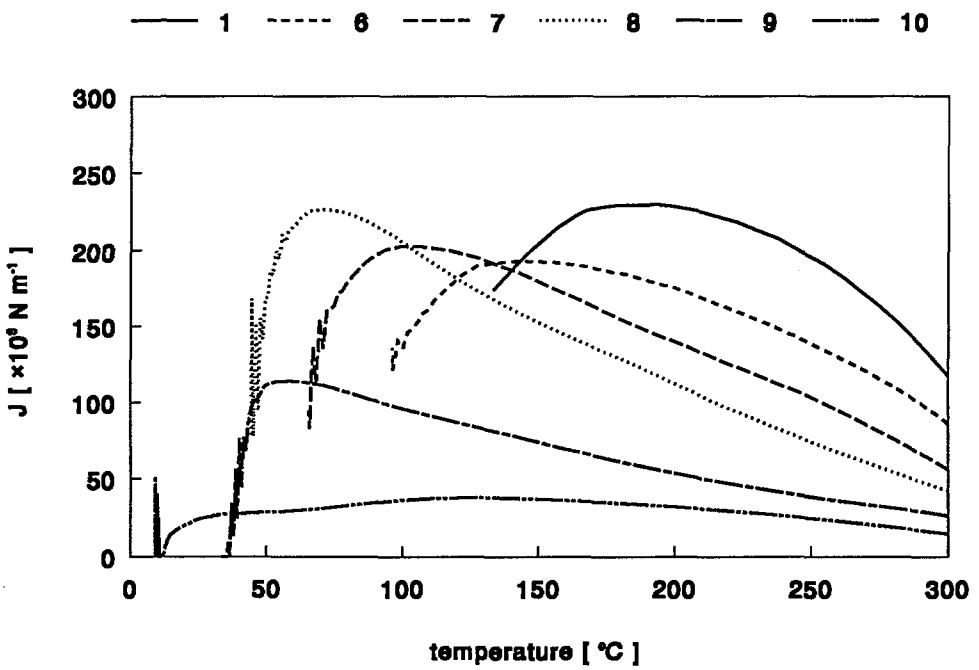

Figure 22 *The spinning cylinder with the surface breaking defect*
The J-integral as a function of temperature for some locations along the crack front (fig. 6) as determined with the elasto-plastic structural analysis

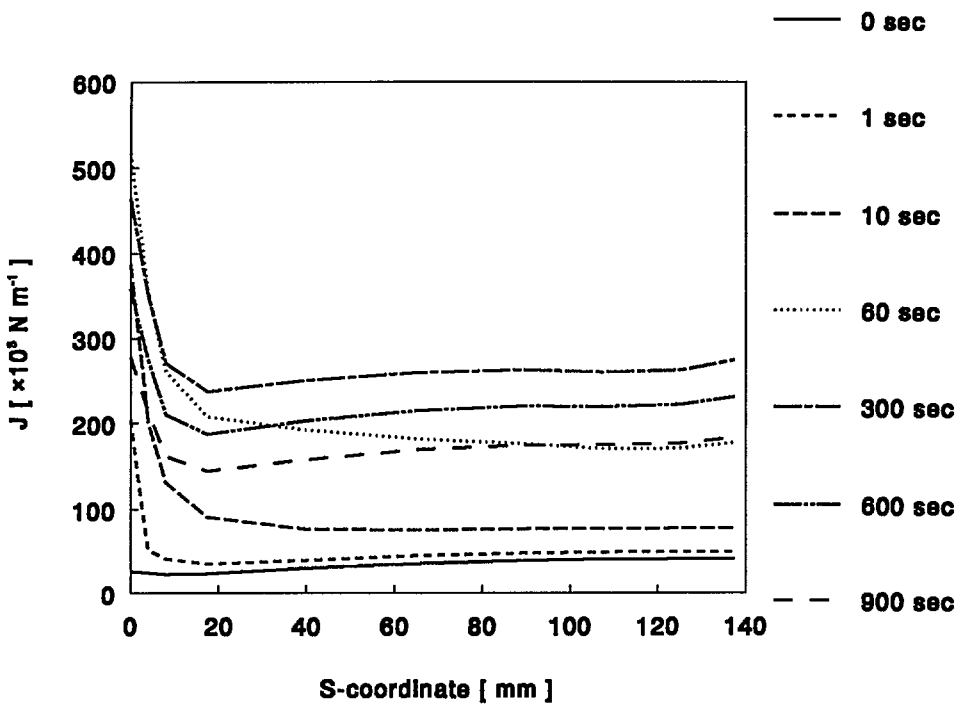

Figure 23 *The spinning cylinder with the surface breaking defect*
The J-integral along the crack front for various points in time as determined with the elastic structural analysis

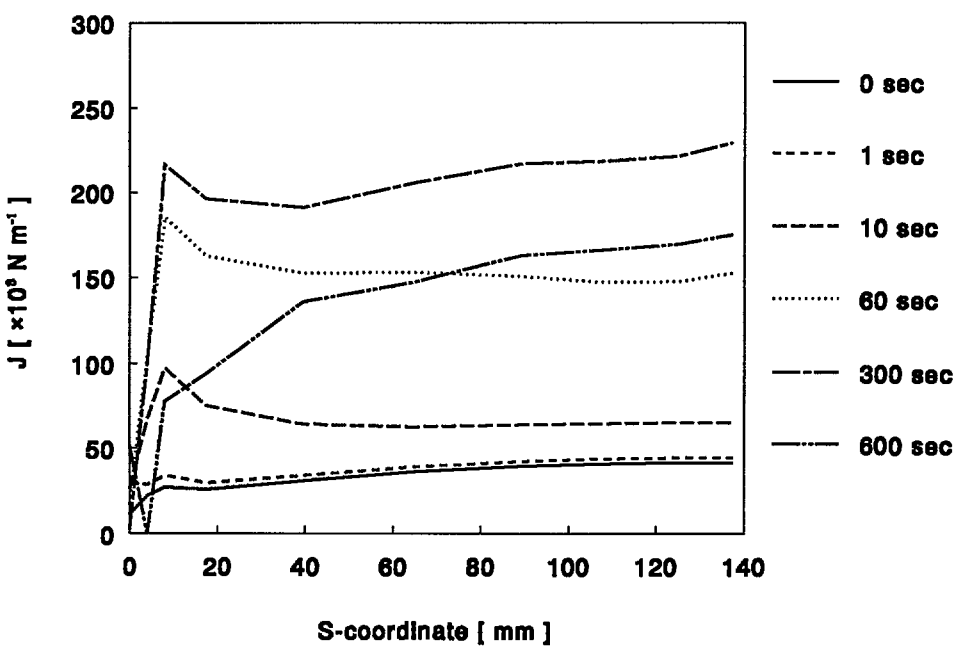

Figure 24 *The spinning cylinder with the surface breaking defect*
The J-integral along the crack front for various points in time as determined with the elasto-plastic structural analysis

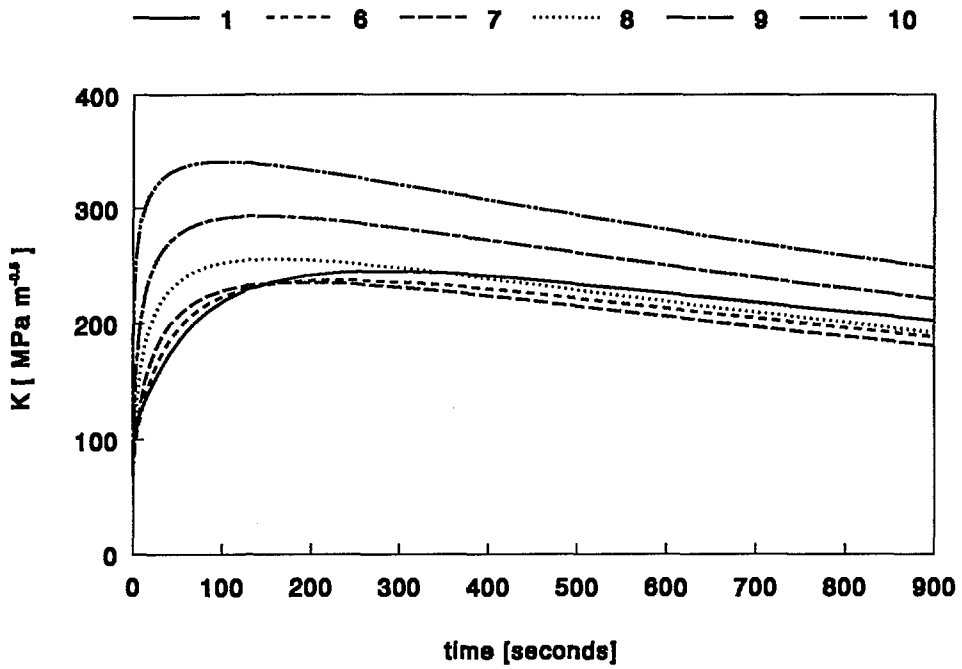

Figure 25 *The spinning cylinder with the surface breaking defect*
The K-factor as a function of time for some locations along the crack front (fig. 6) as determined with the elastic structural analysis

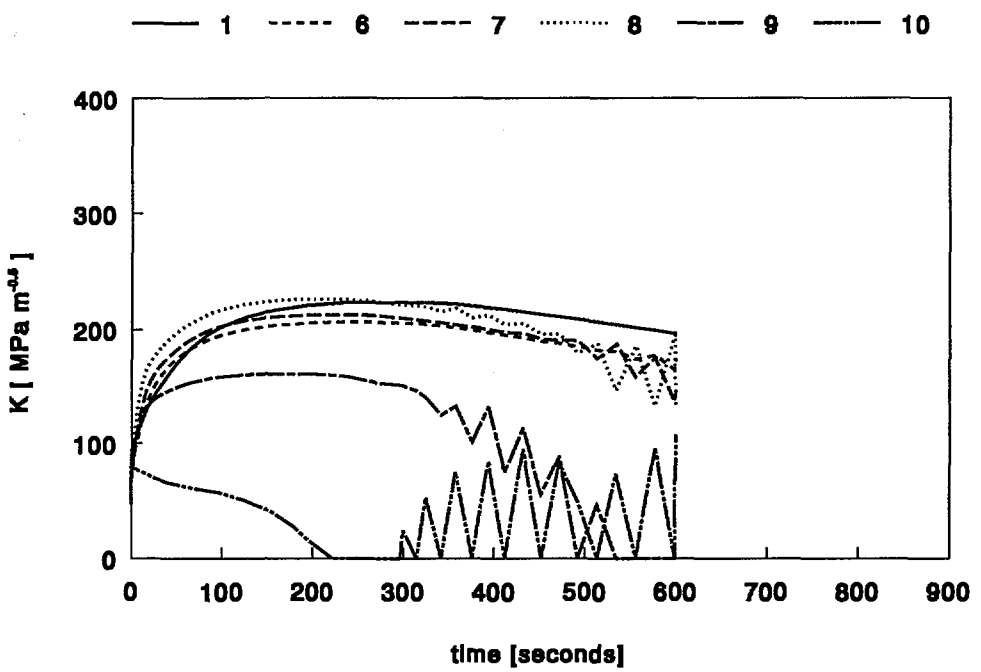

Figure 26 *The spinning cylinder with the surface breaking defect*
The K-factor as a function of time for some locations along the crack front (fig. 6) as determined with the elasto-plastic structural analysis

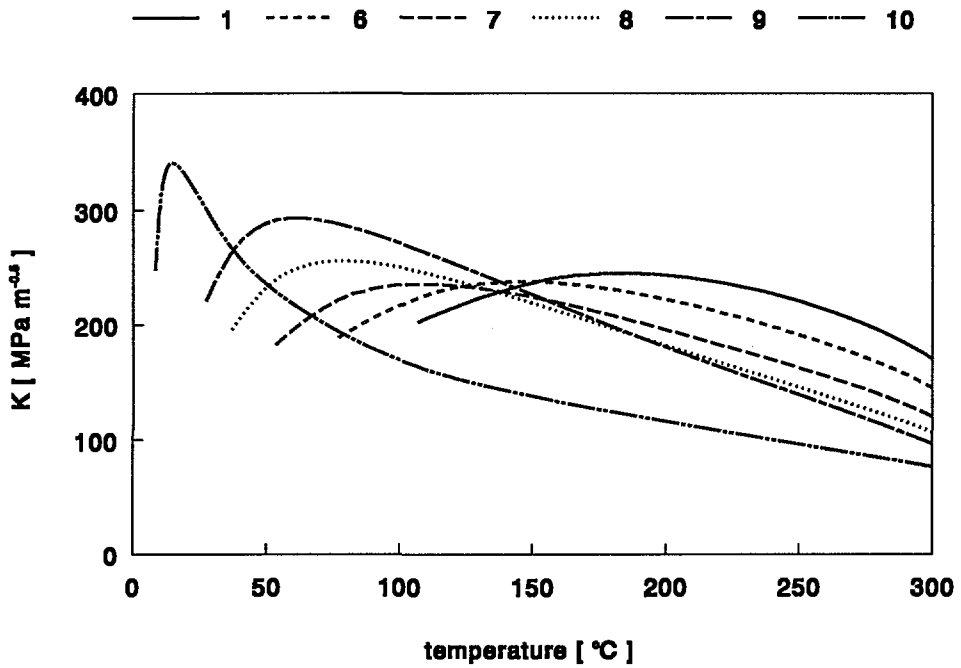

Figure 27 *The spinning cylinder with the surface breaking defect*
The K-factor as a function of temperature for some locations along the crack front (fig. 6) as determined with the elastic structural analysis

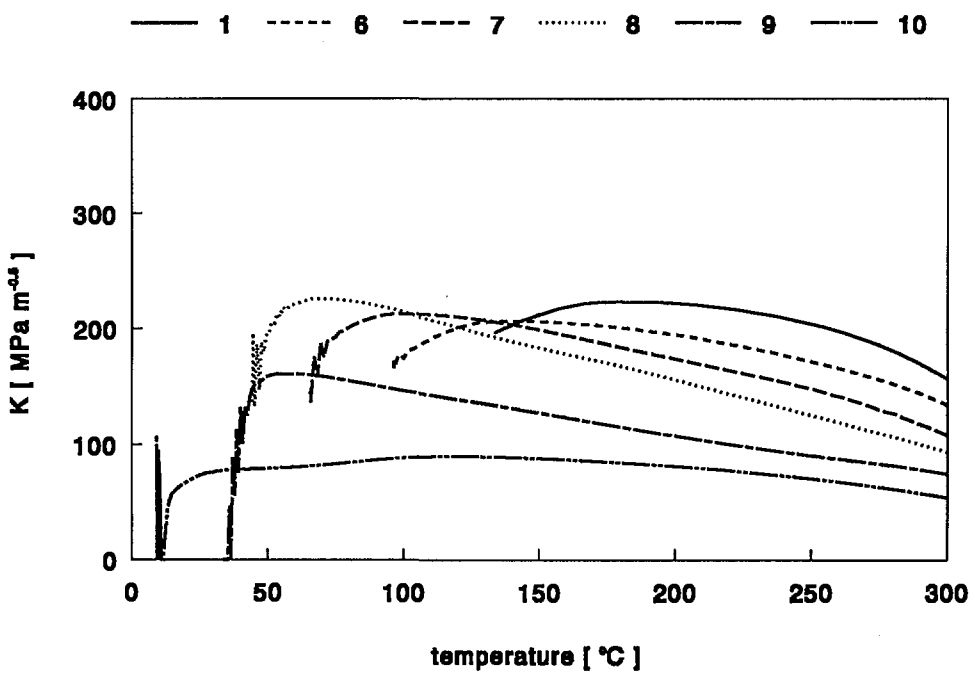

Figure 28 *The spinning cylinder with the surface breaking defect*
The K-factor as a function of temperature for some locations along the crack front (fig. 6) as determined with the elasto-plastic structural analysis

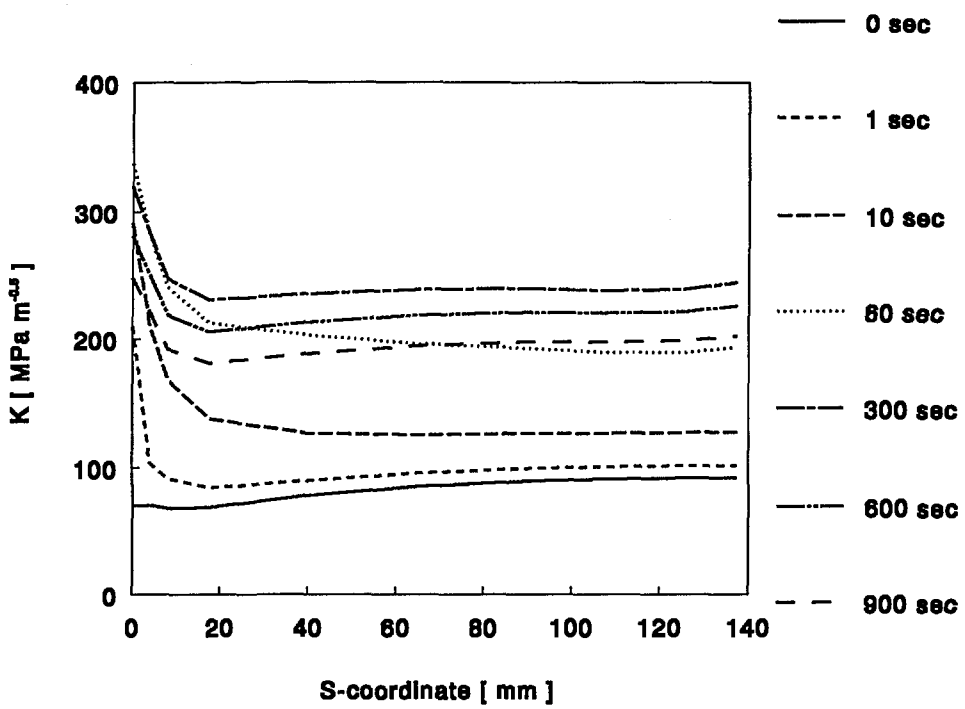

Figure 29 *The spinning cylinder with the surface breaking defect*
The K-factor along the crack front for various points in time as determined with the elastic structural analysis

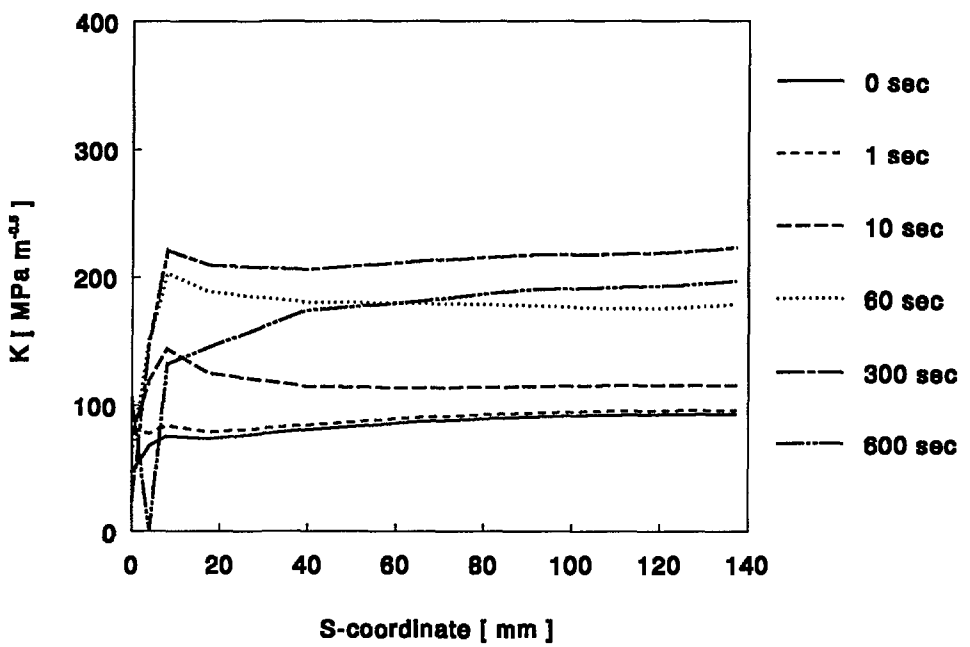

Figure 30 *The spinning cylinder with the surface breaking defect*
The K-factor along the crack front for various points in time as determined with the elasto-plastic structural analysis

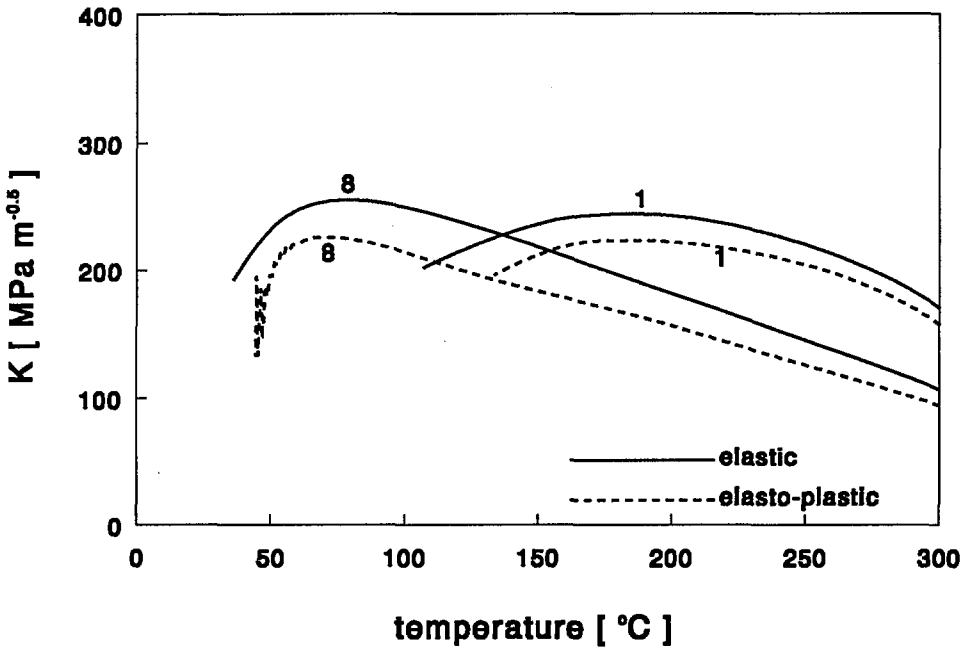

Figure 31 *The spinning cylinder with the surface breaking defect*
The K-factor as a function of temperature in two locations along the crack front depicted in figure 6 as determined with both structural analyses

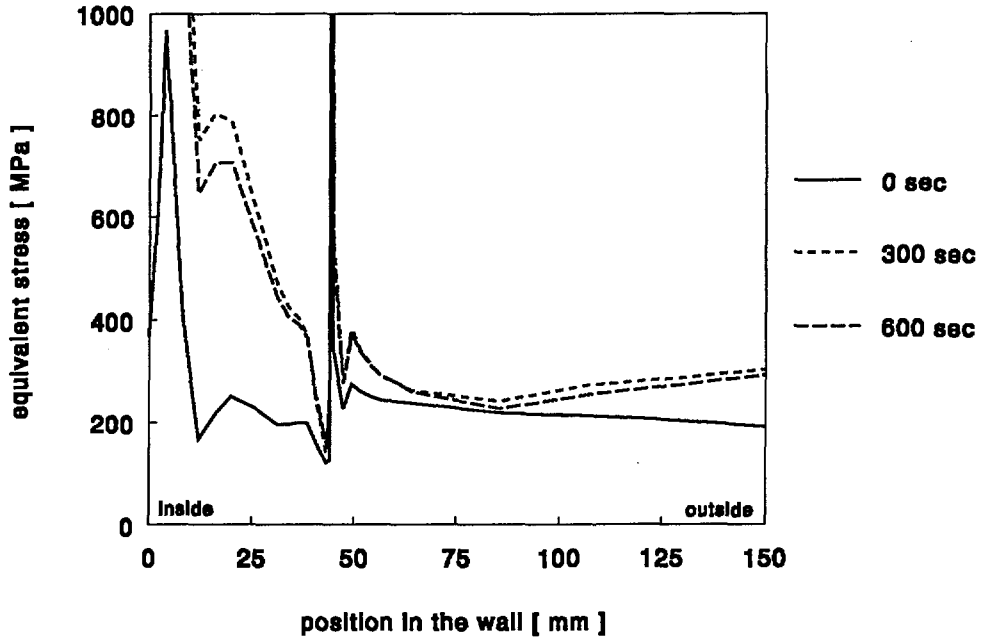

Figure 32 *The spinning cylinder with the subclad defect*
The equivalent stress through the wall thickness for various points in time as determined with the elastic structural analysis

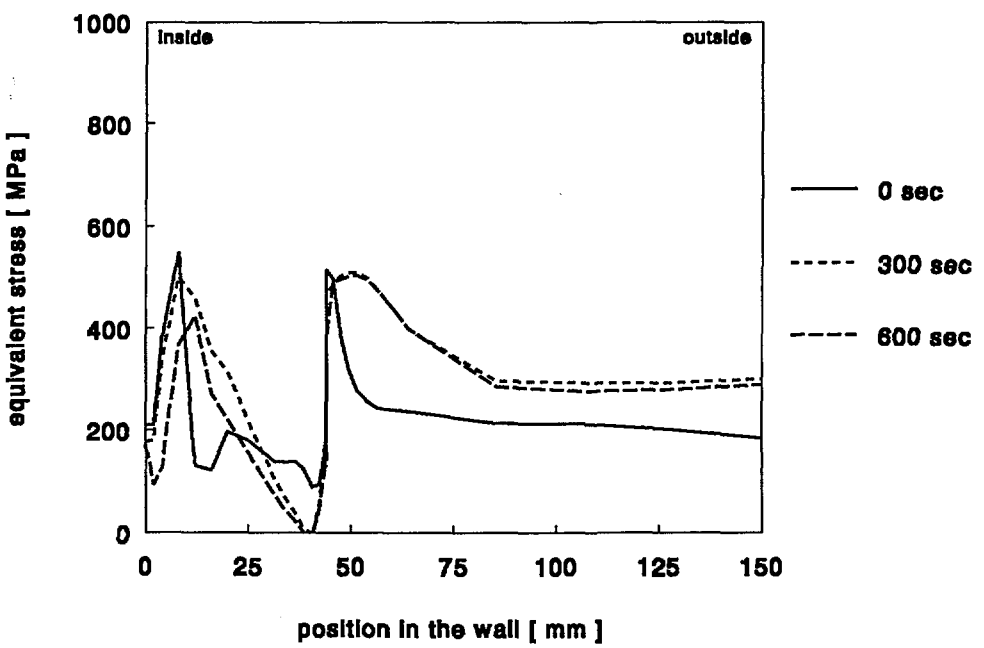

Figure 33 *The spinning cylinder with the subclad defect*
The equivalent stress through the wall thickness for various points in time as determined with the elasto-plastic structural analysis

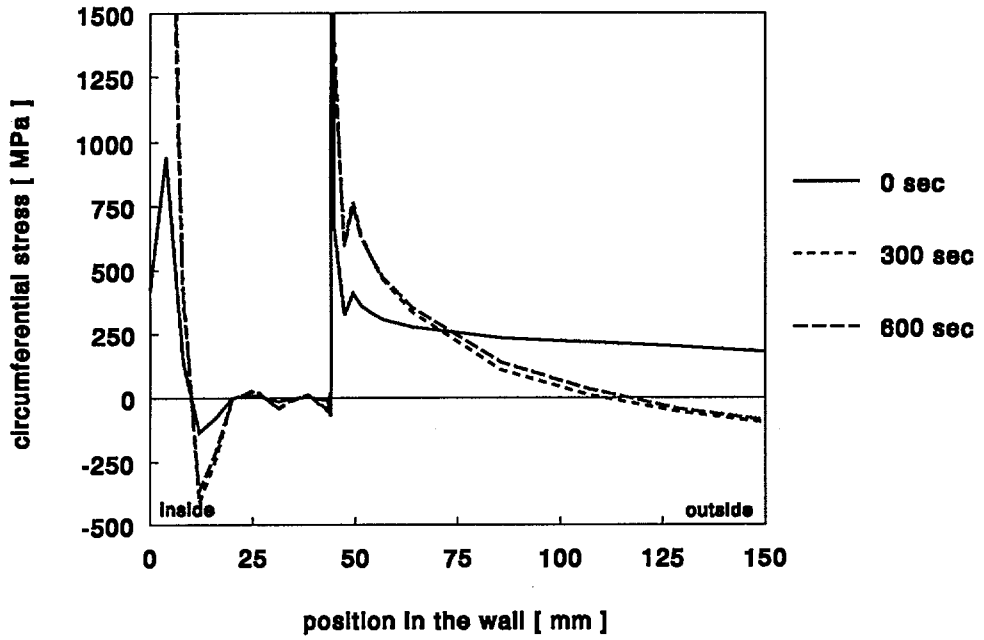

Figure 34 *The spinning cylinder with the subclad defect*
The circumferential stress through the wall thickness for various points in time as determined with the elastic structural analysis

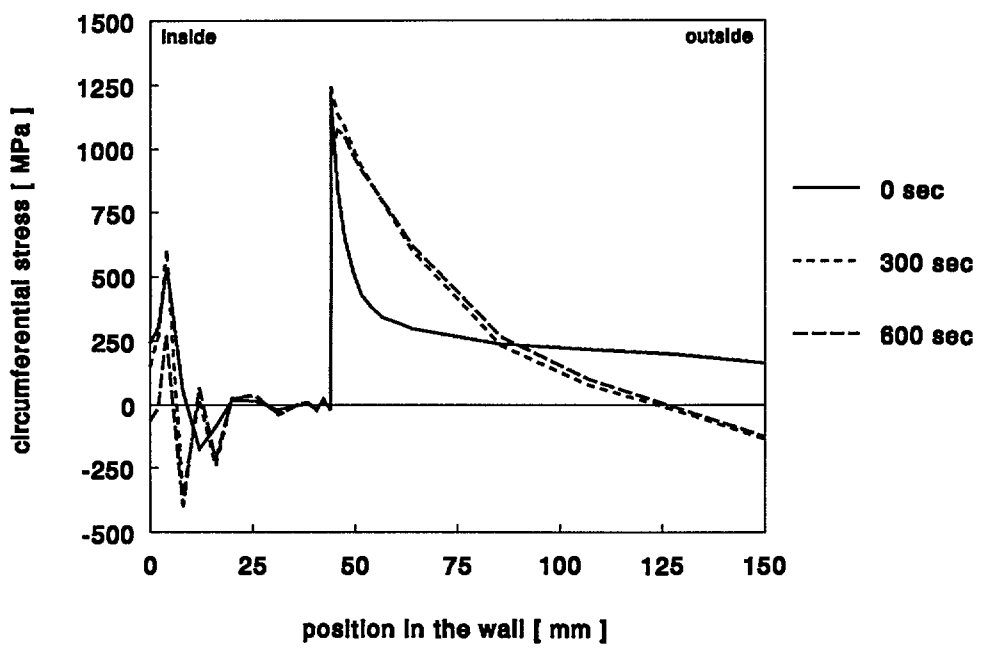

Figure 35 *The spinning cylinder with the subclad defect*
The circumferential stress through the wall thickness for various points in time as determined with the elasto-plastic structural analysis

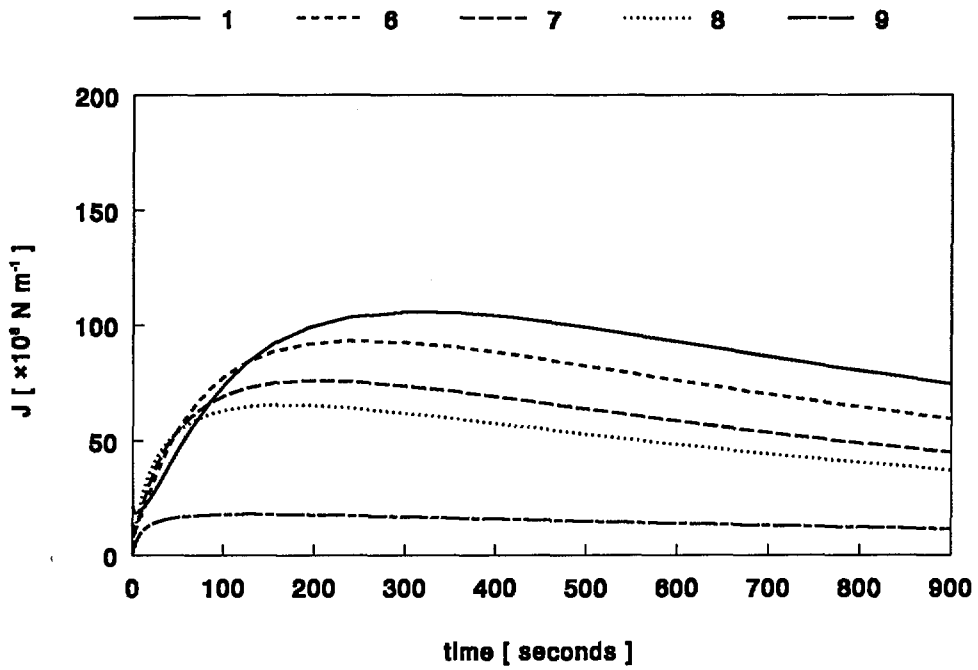

Figure 36 *The spinning cylinder with the subclad defect*
The J-integral as a function of time for some locations along the crack front (fig. 6) as determined with the elastic structural analysis

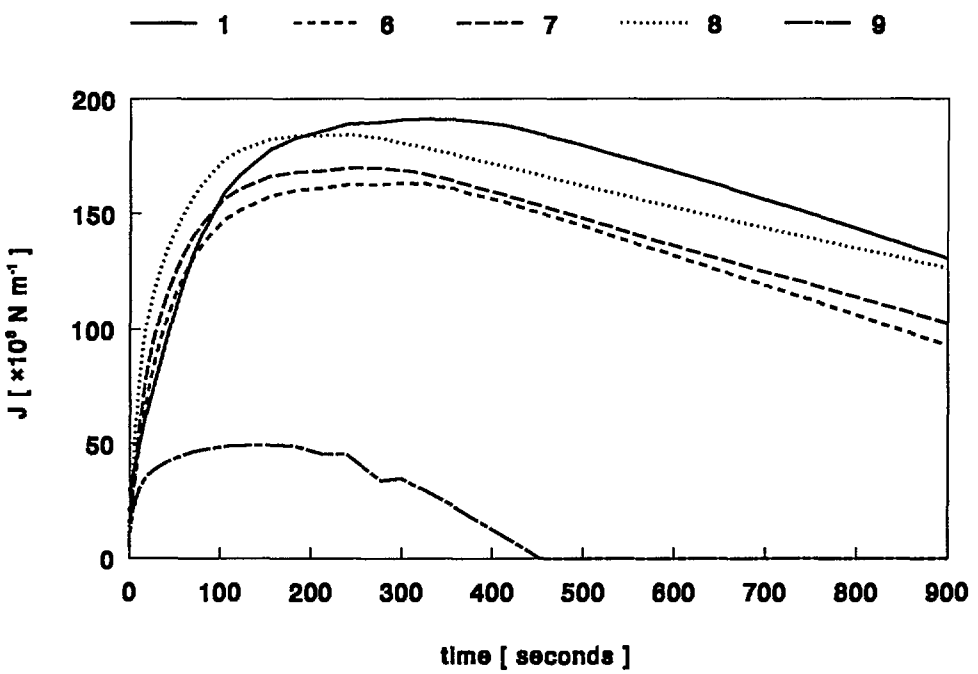

Figure 37 *The spinning cylinder with the subclad defect*
The J-integral as a function of time for some locations along the crack front (fig. 6) as determined with the elasto-plastic structural analysis

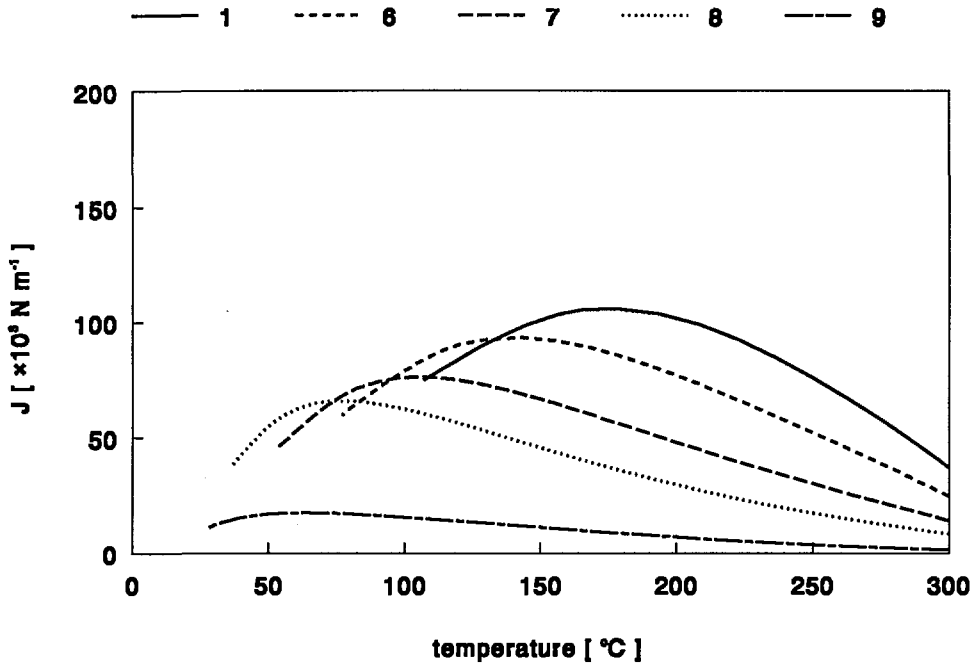

Figure 38 *The spinning cylinder with the subclad defect*
The J-integral as a function of temperature for some locations along the crack front (fig. 6) as determined with the elastic structural analysis

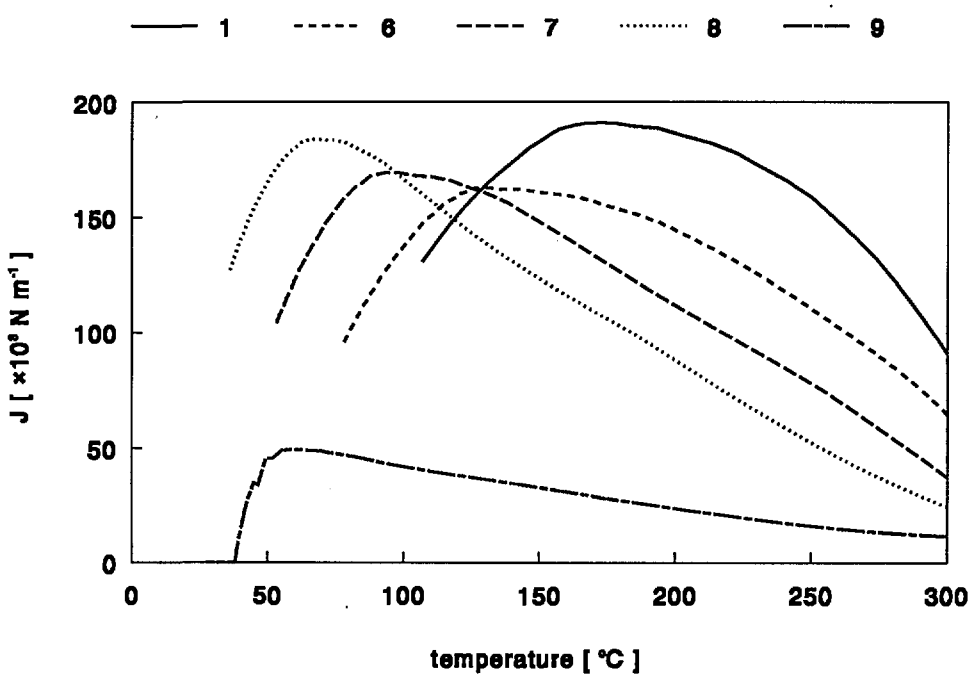

Figure 39 *The spinning cylinder with the subclad defect*
The J-integral as a function of temperature for some locations along the crack front (fig. 6) as determined with the elasto-plastic structural analysis

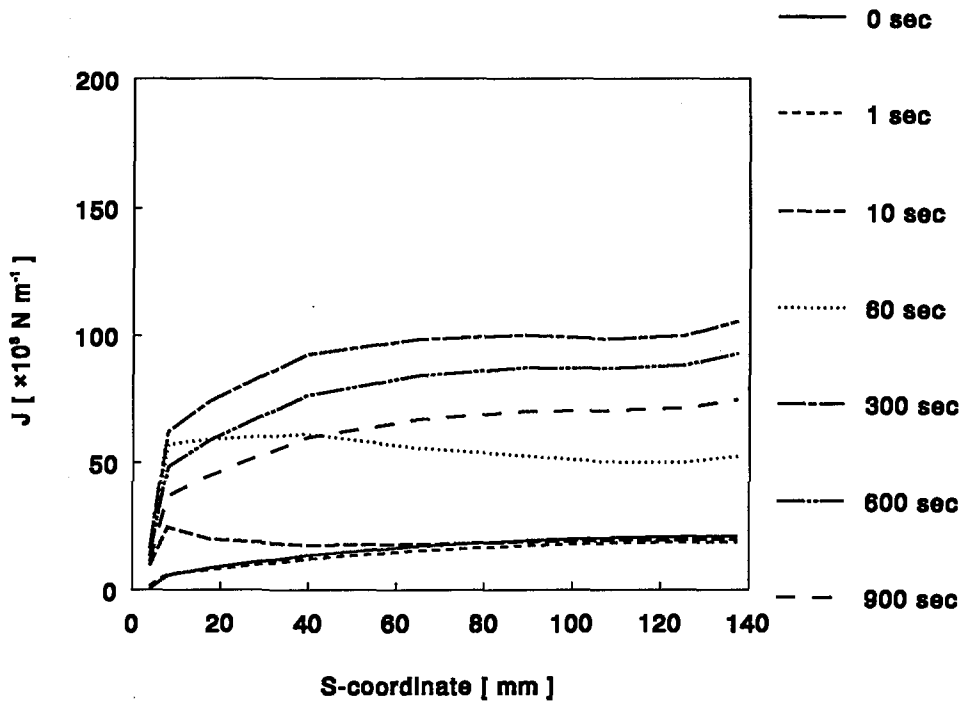

Figure 40 *The spinning cylinder with the subclad defect*
The J-integral along the crack front for various points in time as determined with the elastic structural analysis

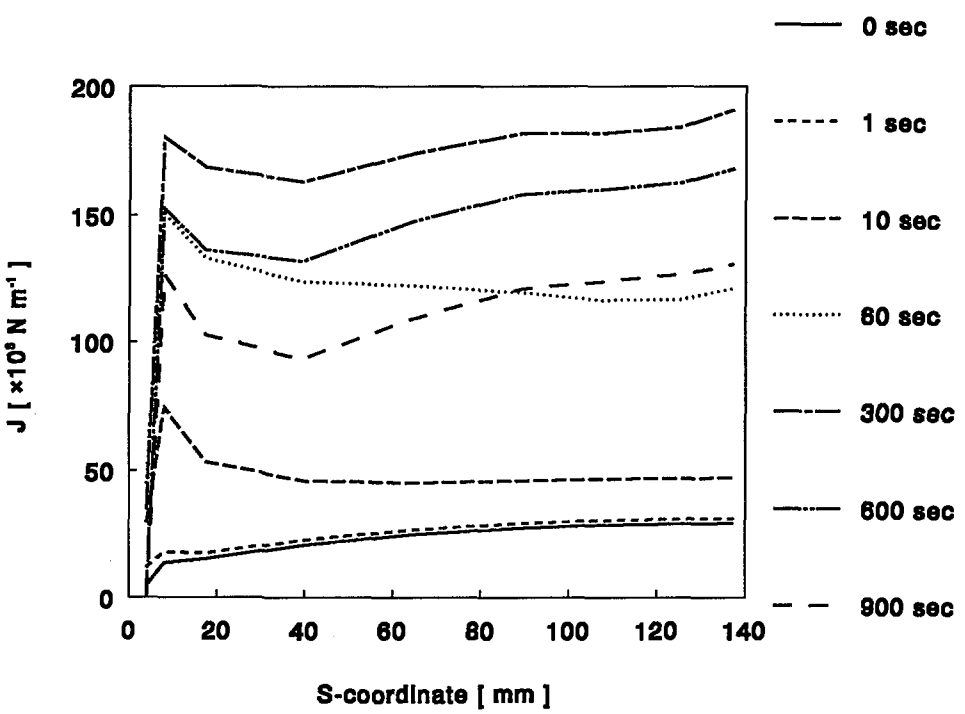

Figure 41 *The spinning cylinder with the subclad defect*
The J-integral along the crack front for various points in time as determined with the elasto-plastic structural analysis

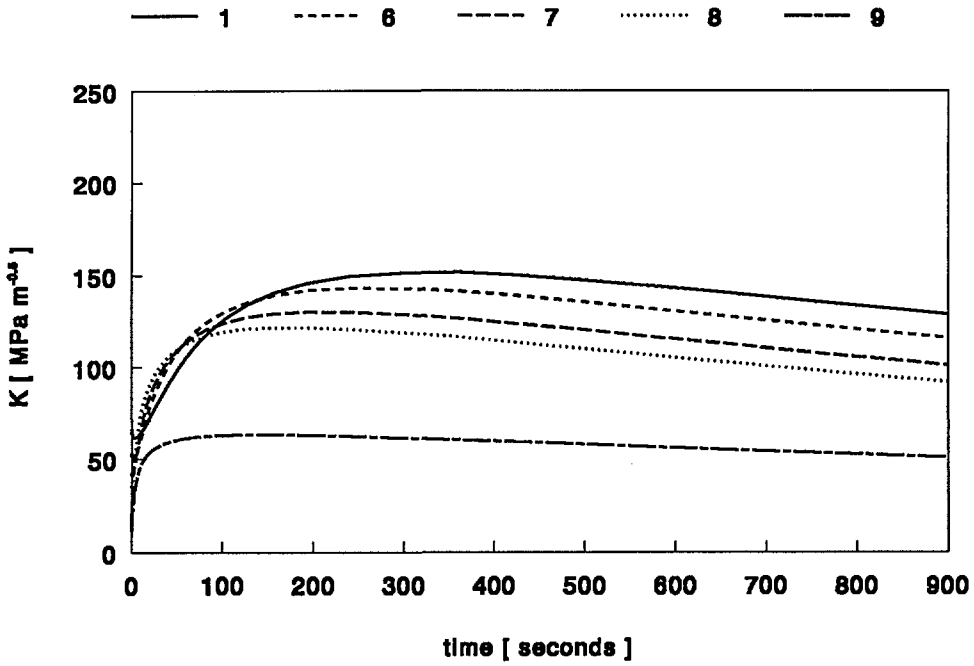

Figure 42 *The spinning cylinder with the subclad defect*
The K-factor as a function of time for some locations along the crack front (fig. 6) as determined with the elastic structural analysis

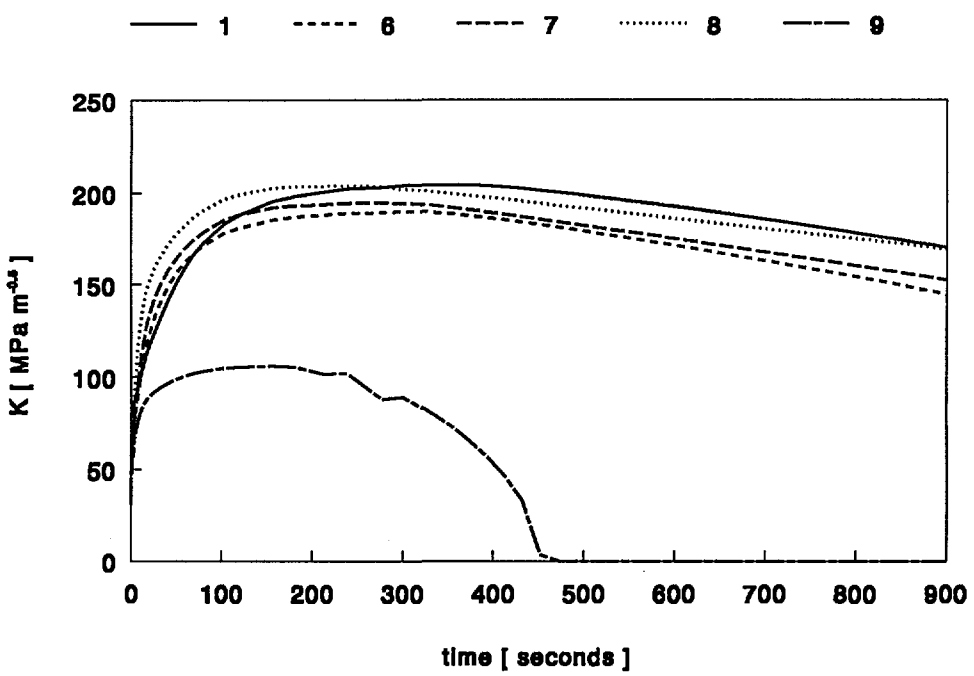

Figure 43 *The spinning cylinder with the subclad defect*
The K-factor as a function of time for some locations along the crack front (fig.6) as determined with the elasto-plastic structural analysis

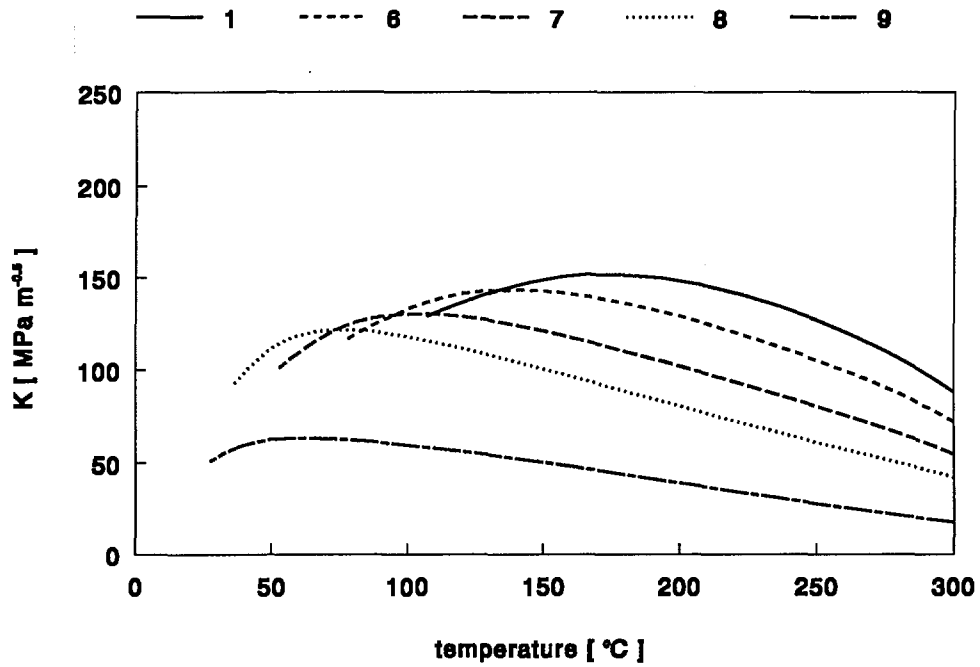

Figure 44 *The spinning cylinder with the subclad defect*
The K-factor as a function of temperature for some locations along the crack front (fig. 6) as determined with the elastic structural analysis

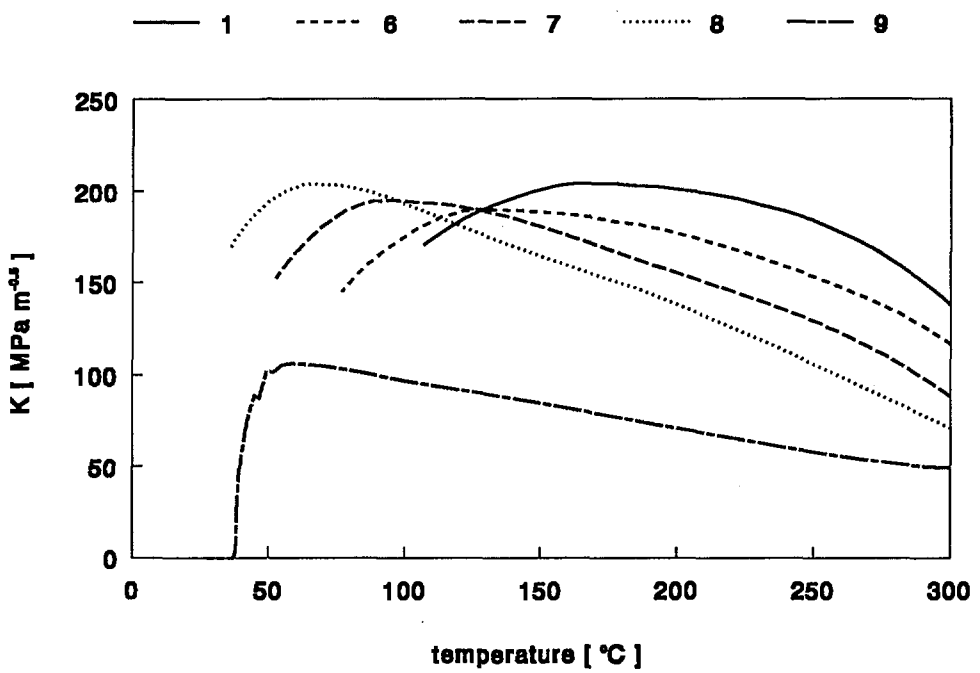

Figure 45 *The spinning cylinder with the subclad defect*
The K-factor as a function of temperature for some locations along the crack front (fig. 6) as determined with the elasto-plastic structural analysis

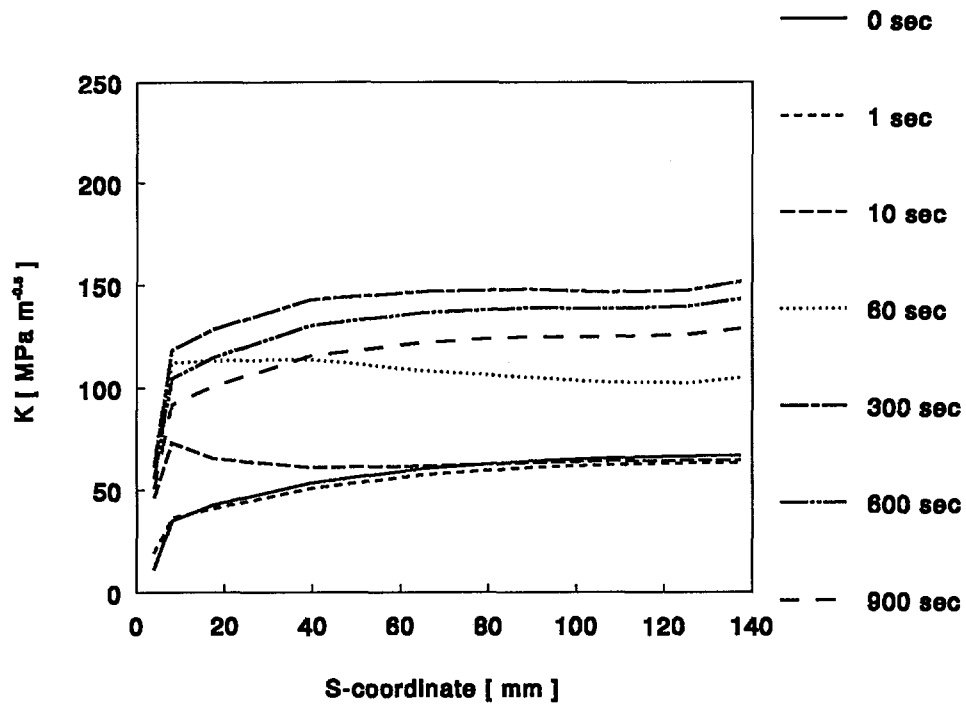

Figure 46 *The spinning cylinder with the subclad defect*
The K-factor along the crack front for various points in time as determined with the elastic structural analysis

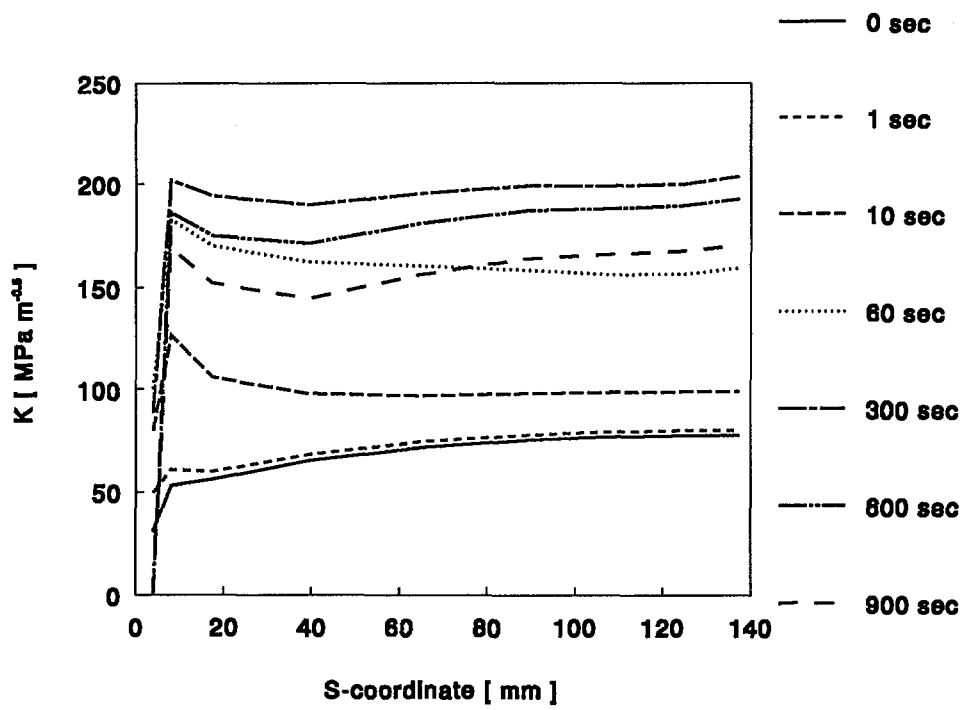

Figure 47 *The spinning cylinder with the subclad defect*
The K-factor along the crack front for various points in time as determined with the elasto-plastic structural analysis

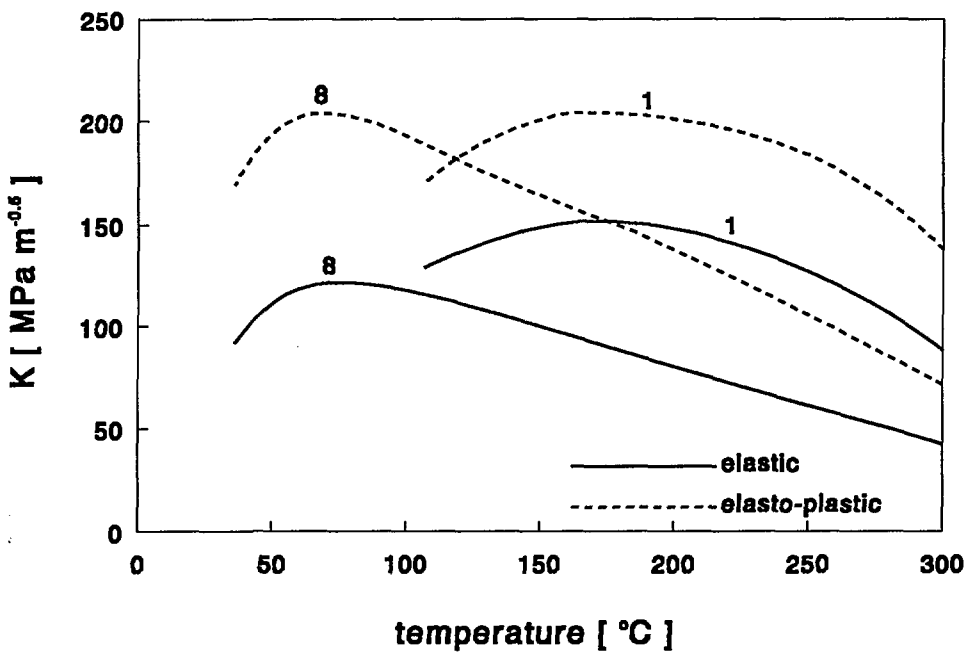

Figure 48 *The spinning cylinder with the subclad defect*
The K-factor as a function of temperature in two locations along the crack front depicted in figure 6 as determined with both structural analyses